JOURNAL OF GUIDANCE, CONTROL, AND DYNAMICS
Vol. 38, No. 12, December 2015

Orbit Estimation of a Continuously Thrusting Spacecraft Using Variable Dimension Filters

Gary M. Goff* and Johnathan T. Black†
U.S. Air Force Institute of Technology, Wright–Patterson Air Force Base, Ohio 45433
and
Joseph A. Beck‡
U.S. Air Force Research Laboratory, Wright–Patterson Air Force Base, Ohio 45433

DOI: 10.2514/1.G001091

The Center for Space Research and Assurance at the U.S. Air Force Institute of Technology investigates short-term tactical spacecraft missions that require frequent maneuvers. An important part of this research is developing methods of performing orbit determination on noncooperative spacecraft that maneuver often at unknown times with unknown thrusts. When a spacecraft performs long-duration thrusts in view of radars, traditional orbit determination, and batch least-squares routines are ineffective methods of fitting the orbit. Adaptive variable-state dimension filters allow for accurate orbit and thrust acceleration estimation during long-duration maneuvers. This work develops and evaluates routines that use both an extended and unscented augmented state Kalman filter along with interacting multiple models to estimate maneuvers. Several methods are evaluated to determine the start and conclusion of continuous maneuvers, and a multiple-model approach is introduced to determine the conclusion of low-thrust continuous maneuvers. Simulation results show that the variable-state dimension interacting multiple model is best at estimating orbits across all thrust levels, whereas a process noise single-model variable-state dimension filter is best when properly tuned for a general thrust magnitude.

Nomenclature

$\boldsymbol{A}$	=	Jacobian
$\boldsymbol{e}$	=	error
el	=	elevation, deg
G	=	observation mapping function
$\boldsymbol{H}$	=	linear/linearized observation matrix
m	=	number of observations in observation vector
n	=	number of states in state vector
$\boldsymbol{P}$	=	covariance
$\hat{\boldsymbol{P}}^s$	=	smoothed covariance
$\underline{\boldsymbol{P}}$	=	interacting multiple-model covariance estimate
$\boldsymbol{Pr}_{j\|k}$	=	interacting multiple-model matrix of jump probabilities
$\boldsymbol{Q}$	=	process noise covariance
$\boldsymbol{R}$	=	observation noise covariance
$\boldsymbol{r}$	=	position, km
$\boldsymbol{S}$	=	predicted observation covariance
th_a	=	thrust acceleration, km/s^2
$\boldsymbol{v}$	=	velocity, km/s
$\boldsymbol{x}$	=	state vector of spacecraft
$\bar{\boldsymbol{x}}$	=	propagated state estimate
$\hat{\boldsymbol{x}}^s$	=	smoother state estimate
$\hat{\boldsymbol{x}}_i^j$	=	state estimate from model j at t_i
$\underline{\boldsymbol{x}}$	=	interacting multiple-model state estimate
$\boldsymbol{y}$	=	observation
$\hat{\boldsymbol{y}}$	=	observation estimate
$\boldsymbol{Z}$	=	smoothing matrix
β	=	azimuth, deg
Θ	=	filter-smoother test, σ standard deviations
$\boldsymbol{\mu}$	=	interacting multiple-model weights
$\boldsymbol{\nu}$	=	residual vector
ρ	=	range, km
$\dot{\rho}$	=	range rate, km/s
ψ_{th}	=	thrust impact scalar
$\Phi(t_f, t_0)$	=	error state transition matrix from initial to final
Ψ	=	maneuver-detection scalar

Presented as Paper 2015-0093 at the AIAA Guidance, Navigation, and Control Conference, Kissimee, FL, 5–9 January 2015; received 1 October 2014; revision received 22 January 2015; accepted for publication 23 January 2015; published online 26 March 2015.

*Graduate Student, 2950 Hobson Way. Member AIAA.
†Professor, Aerospace Engineering, Randolph Hall, RM 203, Virginia Tech, 460 Old Turner Street, Blacksburg, VA 24061. Associate Fellow AIAA.
‡Aerospace Engineer. Senior Member AIAA.

I. Introduction

SPACE is a congested, contested, and competitive environment. The U.S. National Security Space Strategy highlights that space-based assets are vital for conducting military operations [1]. Political pressures and national security postures prevent nations from openly sharing information about the locations and maneuver plans of space assets. This posture emphasizes the need to increase sensor collections and improve techniques to track, predict, and estimate the orbits of noncooperative spacecraft.

To maintain a clear picture of the space environment, the U.S. Air Force (USAF) focuses efforts and resources on the space situational awareness (SSA) mission. SSA is officially defined as "the current and predictive knowledge of the space environment and the operational environment on which space operations depend" [2]. SSA focuses on three basic classes of space objects: noncooperative actively controlled, cooperative actively controlled, and uncontrolled/debris. There are approximately 1000 active spacecraft performing missions in space [3]. These spacecraft maneuver to maintain a mission orbit; unknown maneuvers disrupt the ability of the USAF to accurately track and predict the orbits of these spacecraft. The National Research Council advised the USAF to consider multiple-model adaptive estimation (MMAE) for maneuver detection and specifically mentioned using state-augmented filtering techniques [2]. Although augmented states are often used to measure biases, drag coefficients, or solar radiation pressure [4–6], this research effort develops an adaptive state-augmented filter to track long-duration thrust accelerations.

Statistical orbit determination (SOD) combines the stochastic approaches of minimizing instrument and dynamics model errors with predicting spacecraft orbits and locations [6–8]. The batch least-squares (BLS) filter is used most often by the USAF for determining orbits [2]. This method is chosen because of the sparsity of cataloged

observations for each item tracked. Because over 20,000 objects are tracked as resident space objects [9], only roughly 5% are active spacecraft capable of maneuvering. Therefore, the current tracking mission is mostly associated with uncontrolled object (debris) tracking, in which a few amount of observations are collected, and focus is placed on reducing uncorrelated targets [10].

However, the case is easily made that certain active objects peak interests in the SSA community and warrant more thorough tracking. For high-priority tracking, observation frequencies increase, and a Kalman filter (KF) is able to perform SOD and provide estimation accuracy in the form of a covariance matrix. Recently, interest has grown in adapting the extended Kalman filter (EKF) for use in SOD [11–15]. Additionally, the KF is easily adaptable in state estimation to track additional states. The unscented Kalman filter (UKF) reduces errors associated with the linearized state transition matrix (STM) by propagating points from a probability density function [16,17]. The UKF is gaining popularity as parallelized processing reduces computational time [18,19]. Like most filters, a smoother is applied to improve estimates [20,21].

For real-time tracking problems using sequential filtering, an unplanned change in dynamics (maneuver) may cause filter divergence. To compensate, MMAE approaches are used to handle changes in the dynamics, non-Gaussian noise, and estimate additional state parameters. The fading memory filter is an adaptive method that prevents filter divergence and increases the weight of newer observations through covariance and gain inflation [22–24]. Covariance inflation allows a filter in SOD to converge on a new orbit [25] and proves helpful when changing back and forth between augmented states. The variable-state dimension (VSD) approach uses additional states within the filter to solve for the thrust of an object [26,27]. VSD works well, provided that the thrust occurs for a reasonable length of time and the transition from the nominal filter occurs at the proper time [28,29]. The majority of adaptive tracking of maneuvering object research focuses on linear state propagation in simple coordinate frames and assumes a constant maneuver [30–32]. Input estimation routines limit the tracking approach to a constant maneuver and postprocessing least-squares iteration [33,34]. When maneuver timing is unknown, the suboptimal interacting multiple-model (IMM) approach handles the ambiguity of unknown maneuvers [27,35]. Others have developed smoothers for the IMM [36–38].

Using these techniques for spacecraft tracking requires developing novel algorithms to detect the start and conclusion of maneuvers, leverage covariance inflation to ensure convergence, and tailor process noise to improve performance. This paper formulates an original VSD filter/smoother combination to track a spacecraft performing a continuous-thrust maneuver. Additionally, a varying process noise IMM and fixed epoch smoother are applied within a VSD filter in a new approach to track a continuously maneuvering spacecraft (CMS). The algorithms and analysis developed herein are designed to directly aide the SSA effort in calculating state estimates for CMS.

The paper is organized in the following fashion. Section II provides an overview of the background theory; Sec. III develops the original VSD algorithm for tracking CMS; Sec. IV provides simulation details; Sec. V reviews testing results; and Sec. VI provides relevant conclusions.

II. Background Theory

A. Orbit Determination

Using the state notation, define the state vector of the spacecraft, $\boldsymbol{x}$, as the combination of the position from the center of the Earth to the spacecraft, $\boldsymbol{r}$, and velocity $\boldsymbol{v}$ of the spacecraft in the I, J, K coordinate frame [39]:

$$\boldsymbol{x} = [\, r_I \quad r_J \quad r_K \quad v_I \quad v_J \quad v_K \,]^T \tag{1}$$

Under the influence of Earth's gravity, where μ is Earth's gravitational parameter, and r is the magnitude of the spacecraft position vector; the time derivative of the state and the two-body equations of motion are [39]

$$\dot{\boldsymbol{x}} = \begin{bmatrix} v_I & v_J & v_K & -\frac{\mu r_I}{r^3} & -\frac{\mu r_J}{r^3} & -\frac{\mu r_K}{r^3} \end{bmatrix}^T \tag{2}$$

Using the equation of variation, define the Jacobian matrix $\boldsymbol{A}(t)$ as [39]

$$\boldsymbol{A}(t) = \frac{\partial f(\boldsymbol{x})}{\partial \boldsymbol{x}} = \frac{\partial \dot{\boldsymbol{x}}}{\partial \boldsymbol{x}} = \begin{bmatrix} 0 & \boldsymbol{I} \\ \boldsymbol{\Lambda} & 0 \end{bmatrix} \tag{3}$$

$$\boldsymbol{\Lambda} = \begin{bmatrix} \frac{-\mu}{r^3} + \frac{3\mu r_I^2}{r^5} & \frac{3\mu r_I r_J}{r^5} & \frac{3\mu r_I r_K}{r^5} \\ \frac{3\mu r_I r_J}{r^5} & \frac{-\mu}{r^3} + \frac{3\mu r_J^2}{r^5} & \frac{3\mu r_K r_J}{r^5} \\ \frac{3\mu r_I r_K}{r^5} & \frac{3\mu r_K r_J}{r^5} & \frac{-\mu}{r^3} + \frac{3\mu r_K^2}{r^5} \end{bmatrix} \tag{4}$$

Expanding $\dot{\boldsymbol{x}}$ in a first-order Taylor series and solving the differential equations produces an STM $\boldsymbol{\Phi}(t, t_0)$. The STM propagates based on the differential equation [39]

$$\dot{\boldsymbol{\Phi}}(t_i, t_0) = \boldsymbol{A}(t_i)\boldsymbol{\Phi}(t_i, t_0) \tag{5}$$

with initial conditions that $\boldsymbol{\Phi}(t_0, t_0)$ is the identity matrix $\boldsymbol{I}$. Applying a nondeterministic approach in discrete time and state form at time t_i [40],

$$\bar{\boldsymbol{x}}_{i+1} = F_i \boldsymbol{x}_i + \boldsymbol{w}_i \tag{6}$$

where $\boldsymbol{x}_i$ is the n-dimensional state vector. The bar above $\bar{\boldsymbol{x}}$ represents the state propagated to the next observation, whereas $\hat{\boldsymbol{x}}$ represents the estimate after considering observations at t_i. F_i represents a numerical integration of nonlinear dynamics to update the state variable to the next time step. $\boldsymbol{w}_i$ is the n-dimensional process noise and for zero mean Gaussian noise [40]: $\boldsymbol{w}_i \sim \mathcal{N}(0, \boldsymbol{Q}_i)$. To compare the predicted state to an actual observation, the statistical model of the measurement process is defined as [40]

$$\hat{\boldsymbol{y}}_i = G_i \bar{\boldsymbol{x}}_i + \boldsymbol{v}_i \tag{7}$$

where G_i is the observation mapping function, which transforms the state into a predicted observation; $\hat{\boldsymbol{y}}_i$ is an m-dimensional calculated observation; and $\boldsymbol{v}_i$ is the m-dimensional observation noise: $\boldsymbol{v}_i \sim \mathcal{N}(0, \boldsymbol{R}_i)$ [40].

The error in a state estimate is captured in the state covariance matrix $\boldsymbol{P}$. The covariance provides the confidence in a particular state estimate detailing how the predicted error in the estimate varies. $\boldsymbol{P}_i = E[\, \boldsymbol{e}_i \quad \boldsymbol{e}_i^T \,]$, where $\boldsymbol{e}$ is a vector of length n representing the true error in the state estimate.

Filtering methods are designed to minimize the error between the actual observation and the predicted observation [39]:

$$\boldsymbol{\nu} = \boldsymbol{y}_{\text{ob}} - \boldsymbol{y}_{\text{calc}} = \boldsymbol{y} - \hat{\boldsymbol{y}} \tag{8}$$

where $\boldsymbol{\nu}$ is the m-dimensional residual.

Traditional ground radars tracking spacecraft collect range ρ, azimuth β, elevation el, and range rate $\dot{\rho}$ in the south, east, zenith (SEZ) frame. The transformation of state variables to an observation must include an Earth-central inertial to Earth-centered Earth-fixed (ECEF) rotation, $\text{Rot}_{\text{ECI}\to\text{ECEF}}$, and an ECEF to SEZ coordinate rotation, $\text{Rot}_{\text{ECEF}\to\text{SEZ}}$. The details for the transformations and associated matrices are provided in Appendix A.

Given an initial state estimate, Wiesel [6] and Schutz et al. [7] developed SOD algorithms for the BLS filter and EKF. The BLS filter uses an iterative process to determine the initial covariance matrix at an epoch. The UKF follows a similar process as the EKF but does not linearize the error. Additionally, the output of each KF is improved via a fixed interval smoother that propagates backward in time at the end of a interval [13,41]. This research effort begins with known EKF and UKF approaches and improves the functionality to estimate a CMS.

B. Maneuver Detection

If a spacecraft unknowingly maneuvers and a nominal filter is used to process observations, the residuals in Eq. (8) will reveal a maneuver occurred; the covariance $\boldsymbol{P}$ will not. The filter diverges as residuals grow, and the covariance remains relatively constant. This result is a consequence of mismodeled dynamics, and this work uses new covariance inflation filter-through approaches to prevent filter divergence within a VSD model. A forward-moving maneuver-detection scalar takes advantage of this relationship and declares a maneuver once Ψ grows above a predefined level:

$$\Psi_i = \boldsymbol{\nu}_i^T (\boldsymbol{H}_i \bar{\boldsymbol{P}}_i \boldsymbol{H}_i^T + \boldsymbol{R}_i)^{-1} \boldsymbol{\nu}_i \tag{9}$$

where the variables are defined in Sec. III.B and Appendix A.

Another method to determine spacecraft maneuvers is based on the filter-smoother consistency test [42,43]. The filter-smoother consistency test was originally designed as a method to test the proper amount of process noise covariance during filtering for SOD. The test serves as a method to determine how to properly weight process noise time constants for errors in modeling perturbations, such as drag and solar radiation pressure. Overall, the test determines when a filter approach is properly capturing and modeling the dynamics. Because the filter-smoother test determines whether the orbit is fit properly, it also determines if an unknown maneuver has occurred [44]. If the filter-smoother consistency test suddenly fails after the dynamics were well-modeled and previous estimates passed the test, the time of the failure is the likely start of an unknown maneuver.

The filter-smoother test declares a maneuver using Θ and a known bound. Beginning with the difference between the filter and smoother covariance at time i,

$$\Delta \boldsymbol{P}_i = \hat{\boldsymbol{P}}_i - \hat{\boldsymbol{P}}_i^s \tag{10}$$

Define $\boldsymbol{\sigma}_i$ as a $n \times n$ diagonal matrix composed of indicial notation elements $\sigma_{i_{j,j}}$, which represent the square root of the diagonals in $\Delta \boldsymbol{P}_i$:

$$\sigma_{i_{j,j}} = \sqrt{\Delta \boldsymbol{P}_{i_{j,j}}} \quad \text{for } j = 1, \ldots n \tag{11}$$

where n is the number of states. The difference between the filter state $\hat{\boldsymbol{x}}$ and smoother state $\hat{\boldsymbol{x}}^s$ is used to complete the test:

$$\boldsymbol{\Theta}_i = \boldsymbol{\sigma}_i^{-1} (\hat{\boldsymbol{x}}_i - \hat{\boldsymbol{x}}_i^s) \tag{12}$$

$\boldsymbol{\Theta}_i$ is a vector of length n that determines whether all states are properly estimated or if a maneuver has occurred. A maneuver is declared at t_i if the absolute value of any of the elements Θ in the vector $\boldsymbol{\Theta}_i$ exceed a set threshold. During simulation testing, Θ describes the largest element in $\boldsymbol{\Theta}$ at each time. In this work, the filter-smoother test is adapted for the use of maneuver detection, and its performance is evaluated for detecting the start and stop of small continuous thrusts.

III. Adaptive Variable-State Dimension Filter

Increasing the filter's covariance provides a method for the filter to reconverge on the new orbital solution. When tracking a high-priority CMS, it is assumed that the postmaneuver observations are known to pertain to the target. In this case, filtering through unknown maneuvers requires detecting the maneuver then inflating the covariance to compensate for unknown dynamics changes. This method is similar to an abrupt fading memory filter [23]. Improving the traditional EKF and UKF tracking routines to inflate the covariance after a maneuver is detected allows the filters to continue processing observations and tracking the spacecraft as time progresses.

Nominal methods of spacecraft tracking consider a maneuver as the start of a new orbit, in which case a new initial orbit process attempts to fit the postmaneuver orbit. These approaches along with other initial orbit determination (IOD) methods are designed to converge on a new postmaneuver orbit; however, in the continuous-thrust case, the spacecraft is still maneuvering and the orbit is still changing. The filter attempts to converge to an orbit that is changing at each observation step. Additionally, the same issue occurs when a nominal BLS approach is used to update an epoch during a continuous-thrust period. If the BLS converges in the first place, the new epoch will consist of some averaged state errors caused by the maneuver. If the BLS output state epoch is propagated using a nominal EKF, the filter will quickly diverge. Clearly, a different approach is required, and the key is extending and adapting maneuver target tracking schemes designed for linear systems (i.e., aircraft) to the nonlinear discrete dynamic cases for SSA. The maneuver detection and covariance inflation approach allows a VSD to smoothly transition between added state variables.

For the continuous-thrust case, the VSD filter prevents filter divergence. After a maneuver is detected when either Ψ or Θ is larger than a set tolerance, the state variable is augmented to estimate a thrust acceleration vector:

$$\boldsymbol{x}_{\text{Add}} = [\, r_I \quad r_J \quad r_K \quad v_I \quad v_J \quad v_K \quad \text{th}_{a_I} \quad \text{th}_{a_J} \quad \text{th}_{a_K} \,]^T \tag{13}$$

where th_a estimates the components of the thrust acceleration for the maneuver. Also, the covariance must increase in size to account for the new variables:

$$\boldsymbol{P}_{\text{Add}} = \begin{bmatrix} \boldsymbol{P} & 0 \\ 0 & \boldsymbol{P}_{\text{th}_a} \end{bmatrix} \tag{14}$$

where $\boldsymbol{P}_{\text{th}_a}$ is a 3×3 matrix containing the error in estimating the thrust. To estimate the new states, it is necessary to include them in the dynamics function:

$$\dot{\boldsymbol{x}}_{\text{Add}} = \begin{bmatrix} v_I & v_J & v_K & -\frac{\mu r_I}{r^3} + \text{th}_{a_I} & -\frac{\mu r_J}{r^3} + \text{th}_{a_J} & -\frac{\mu r_K}{r^3} + \text{th}_{a_K} & 0 & 0 & 0 \end{bmatrix}^T \tag{15}$$

For the EKF, the error state transition matrix equation [Eq. (5)] and Jacobian [Eq. (3)] are updated to account for the added states:

$$\boldsymbol{A}_{\text{Add}}(t) = \frac{\partial \dot{\boldsymbol{x}}_{\text{Add}}}{\partial \boldsymbol{x}_{\text{Add}}} = \begin{bmatrix} 0 & \boldsymbol{I} & 0 \\ \boldsymbol{\Lambda} & 0 & \boldsymbol{I} \\ 0 & 0 & 0 \end{bmatrix} \tag{16}$$

where each element is a 3×3 matrix. The mapping function from one frame to the next is not changed because the thrust state variables are not used after the integration when estimating the observations. In the UKF, it is also important to update the number of states $n = 9$ in the algorithm and verify that weights and summations are calculated properly.

The thrust acceleration vector th_a is purposefully selected as the additional states to generalize the approach. If $\Delta \boldsymbol{v}$ is selected as a state, the calculation becomes less general as defining masses and engine performance is required. The thrust acceleration state allows for calculating the maneuver as additional accelerations experienced by the spacecraft that are not modeled within the dynamics. This approach works best when the perturbing accelerations of the orbit are well known and estimated. For the scenarios, two-body equations are used, but the approach is directly applicable to any higher-order propagator and estimation routine that accounts for perturbations.

When transitioning between state variables with different lengths, it is important to account for the times the transitions are made. The smoothing of the augmented filter outputs and nominal filter outputs must occur separately. Because of the change in size of the state, covariance, and error state transition matrices, the smoother operations cannot occur across a transition between different state variable sizes. The algorithms must track the start and stop of the additional states and store this information when determining smoothing intervals.

While estimating an unobservable thrust acceleration, the filter can at times grow overconfident in the estimate and diverge with large residuals and large Ψ values, falsely indicating the possible conclusion of the maneuver. Improving the VSD filter is possible by tuning

the filter with added uncertainty in the form of $\boldsymbol{Q}$ as defined in Sec. II.A. Define $\boldsymbol{Q}_{\text{Add}}$ as a 9×9 diagonal matrix composed of three 3×3 diagonal matrices with scalar values of $\boldsymbol{Q}_r, \boldsymbol{Q}_v, \boldsymbol{Q}_{\text{th}}$. The values are separated to scale constants for the added uncertainty during the estimation of the position, velocity, and thrust. $\boldsymbol{Q}$ is nominally used to model propagation errors but is tunable to improve filter performance during thrust estimation. Applying the VSD to tracking CMS requires understanding and using added process noise to improve performance.

In the VSD approach, it is important to only estimate the thrust when the spacecraft is thrusting; otherwise, the filter estimate is less accurate. If the approach is delayed in determining the start of the maneuver, errors build up as the spacecraft of interest maneuvers. If the conclusion of the maneuver is not detected, the filter miscategorizes orbit errors as potential thrust accelerations causing errors to build. The start of the thrust is determined using Ψ in Eq. (9) and Θ in Eq. (12), and the conclusion of the thrust is possible (at times) to determine using the exact same method. While estimating the additional states during maneuvers, once Ψ or Θ exceeds a limit, the maneuver is declared complete. To use Ψ or Θ, the conclusion of the maneuver must cause errors large enough for the methods to detect.

Besides Ψ and Θ, there are other methods to determine the conclusion of the thrust. The thrust estimated as additional states during the maneuver decreases when the spacecraft concludes the maneuver. A simple way to determine the end of the maneuver is to just look at the magnitude of the estimated thrust from the VSD filter, $|\text{th}_a|_2$. Once the thrust magnitude dips into the noise floor, the maneuver is declared over. This approach is typically slow in determining the conclusion of the thrust but is fairly obvious if the filter is properly tuned. Another method to determine the conclusion of the thrust uses a very similar approach to Ψ, but instead only the thrust components are considered [27]:

$$\psi_{\text{th}} = \text{th}_a^T (\boldsymbol{P}_{\text{th}_a})^{-1} \text{th}_a \tag{17}$$

ψ_{th} highlights (in the form of a scalar) when the estimated thrust is insignificant and the maneuver has concluded. Once below a threshold, ψ_{th} indicates the end of the maneuver. Each method performs differently when the size of the maneuver is varied as detailed in Sec. V.

A. Multiple-Model Estimation of End of Continuous Thrust

In the single-model approach, when the thrust acceleration magnitude is too small to determine the end of the maneuver by examining ψ_{th} or $|\text{th}_a|_2$, a novel multiple-model approach is developed. The approach originated under necessity because all reviewed methods for a single VSD filter continued to estimate thrust states long after the conclusion of the maneuver resulting in increased errors. Figure 1 shows the strategy for determining maneuver termination. The multiple-model approach leverages the fact that Ψ indicates in real time whether or not the filter outputs fit the orbit. Thus, if Ψ remains below a threshold when a nominal filter is run, the maneuver has ended. Similarly, Θ is another measure to use in the multiple-model approach to provide a near-real-time estimate of the conclusion of the thrust (with a slight delay due to the backward running smoother).

The multiple-model approach to determine the conclusion of a maneuver allows for starting nominal filters as often as accuracy requirements demand. It is necessary to inflate the covariance during the transition because it is unlikely that the orbit is perfectly estimated at the time. Next, the nominal filter will attempt to lower the covariance and converge on an orbit. If the spacecraft is not maneuvering, the filter will converge on the new orbit, and Θ and Ψ will remain below their respective thresholds. However, if the conclusion is estimated prematurely, the filter will diverge as indicated by Θ and Ψ. For the approach to work, each estimate of the end of the maneuver must run for a period of time after the covariance is lowered to determine the accuracy of the prediction. The multiple-model VSD approach provides a method to estimate, in real time and near real time, the end of small-magnitude continuous maneuvers using a single model. Without an effective method to determine the conclusion of the thrust, the estimation routine continues to incorrectly estimate a thrust state and the accuracy of the solution is continually poor.

B. Variable-State Dimension Tracking Filters for Maneuvering Spacecraft

Using techniques of Kalman and VSD filtering for spacecraft tracking, this section details the logic to track a CMS. This new approach adapts the VSD filter concept for use in the spacecraft tracking problem by using covariance inflation, process noise, and estimating thrust dynamics. Additionally, the filter is adaptable to use any of the maneuver start detection and maneuver end detection methods discussed in the previous sections. This algorithm differs from traditional VSD models because it requires covariance inflation after increasing the size of the state vector to converge on the CMS. The UKF version of the adaptive VSD filter preserves the logic in Sec. III.B, except that the UKF equations are used to estimate the state and covariance. To implement the UKF, use the standard UKF [16,17] propagation and estimation routines along with the logic discussed shortly. The algorithm extends and improves existing filtering methods in the literature from their generic forms into a method to meet the SSA demands for tracking a high-priority noncooperative spacecraft.

Begin by defining or updating a previous covariance and state reference, $\hat{\boldsymbol{P}}_0$ and $\hat{\boldsymbol{x}}_0$. Then, read in the next observation: t_i, $\boldsymbol{y}_i$, $\boldsymbol{R}_i$. Next, propagate the state from t_{i-1} to t_i using numerical integration of the dynamics:

$$\dot{\boldsymbol{x}} = f(\boldsymbol{x}, t) \tag{18}$$

$$\dot{\boldsymbol{\Phi}} = \left[\frac{f(\boldsymbol{x}, t)}{\partial \boldsymbol{x}}\right] \boldsymbol{\Phi}(t, t_{i-1}) \tag{19}$$

The initial conditions of the integration are $\hat{\boldsymbol{x}}_{i-1}$ and $\boldsymbol{\Phi}(t_{i-1}, t_{i-1}) = \boldsymbol{I}$. The results of the integration are $\bar{\boldsymbol{x}}_i$ and $\boldsymbol{\Phi}(t_i, t_{i-1})$. The propagated covariance is defined as

$$\bar{\boldsymbol{P}}_i = \boldsymbol{\Phi}(t_i, t_0) \hat{\boldsymbol{P}}_{i-1} \boldsymbol{\Phi}(t_i, t_0)^T + \boldsymbol{Q}_i \tag{20}$$

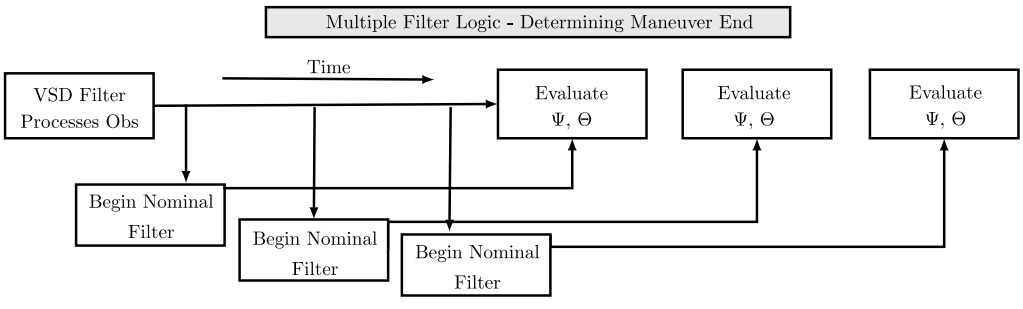

Fig. 1 Multiple-model estimate of maneuver conclusion using Ψ and Θ.

Next, find partial derivatives and determine residuals:

$$\boldsymbol{H}_i = \left[\frac{\partial G(\bar{\boldsymbol{x}}_i, t)}{\partial \boldsymbol{x}}\right] \tag{21}$$

$$\boldsymbol{\nu}_i = \boldsymbol{y}_i - G(\bar{\boldsymbol{x}}_i, t_i) \tag{22}$$

Then, calculate the observation covariance:

$$\boldsymbol{S}_i = \boldsymbol{H}_i \bar{\boldsymbol{P}}_i \boldsymbol{H}_i^T + \boldsymbol{R}_i \tag{23}$$

The maneuver-detection scalar Ψ is defined as

$$\Psi_i = \boldsymbol{\nu}_i^T (\boldsymbol{S}_i)^{-1} \boldsymbol{\nu}_i \tag{24}$$

Use the traditional Kalman gain derivation to estimate the state and covariance:

$$\boldsymbol{K}_i = \bar{\boldsymbol{P}}_i \boldsymbol{H}_i^T (\boldsymbol{S}_i)^{-1} \tag{25}$$

$$\hat{\boldsymbol{x}}_i = \bar{\boldsymbol{x}}_i + \boldsymbol{K}_i \boldsymbol{\nu}_i \tag{26}$$

$$\hat{\boldsymbol{P}}_i = (\boldsymbol{I} - \boldsymbol{K}_i \boldsymbol{H}_i) \bar{\boldsymbol{P}}_i \tag{27}$$

Once a maneuver is initially detected (Ψ_i is greater than the maneuver threshold), increase the states to estimate the thrust:

$$\hat{\boldsymbol{x}}_i = \boldsymbol{x}_{\text{Add}} = [\, r_I \quad r_J \quad r_K \quad v_I \quad v_J \quad v_K \quad 0 \quad 0 \quad 0 \,]^T \tag{28}$$

Simultaneously, add dimensions to the covariance:

$$\hat{\boldsymbol{P}}_i = \boldsymbol{P}_{\text{Add}} = \begin{bmatrix} \boldsymbol{P}_{rr} & \boldsymbol{P}_{rv} & 0 \\ \boldsymbol{P}_{vr} & \boldsymbol{P}_{vr} & 0 \\ 0 & 0 & \boldsymbol{P}_{vv} \end{bmatrix} \tag{29}$$

Also, inflate the covariance until the trace ($\hat{\boldsymbol{P}}_i$) is less than the inflation threshold by repeating the operation

$$\hat{\boldsymbol{P}}_i = 10\hat{\boldsymbol{P}}_i \tag{30}$$

Once the maneuver concludes, reduce dimensions:

$$\hat{\boldsymbol{x}}_i = [\, r_I \quad r_J \quad r_K \quad v_I \quad v_J \quad v_K \,]^T \tag{31}$$

$$\hat{\boldsymbol{P}}_i = \begin{bmatrix} \boldsymbol{P}_{rr} & \boldsymbol{P}_{rv} \\ \boldsymbol{P}_{vr} & \boldsymbol{P}_{vv} \end{bmatrix} \tag{32}$$

Also, inflate the covariance again using Eq. (30). After processing an interval of observations, filter estimates are improved with a smoother. Set $i = N$ at $t_i = t_N$, where N is the last observation of the pass. Set $\hat{\boldsymbol{P}}_N^s = \hat{\boldsymbol{P}}_N$ and $\hat{\boldsymbol{x}}_n^N = \hat{\boldsymbol{x}}_N$. Solve for the smoothed state and covariance at each observation using the equations

$$\boldsymbol{Z} = \hat{\boldsymbol{P}}_{i-1} \boldsymbol{\Phi}(t_i, t_{i-1}) \bar{\boldsymbol{P}}_i^{-1} \tag{33}$$

$$\hat{\boldsymbol{x}}_{i-1}^s = \hat{\boldsymbol{x}}_{i-1} + \boldsymbol{Z}(\hat{\boldsymbol{x}}_i^s - \bar{\boldsymbol{x}}_i) \tag{34}$$

$$\hat{\boldsymbol{P}}_{i-1}^s = \hat{\boldsymbol{P}}_{i-1} + \boldsymbol{Z}(\hat{\boldsymbol{P}}_i^s - \bar{\boldsymbol{P}}_i)\boldsymbol{Z}^T \tag{35}$$

Continue working backward until all observations in the interval are processed and $t_{i-1} = t_0$. Ensure state dimensions are consistent throughout the smoothing interval when transitioning between maneuvering and nominal estimation.

C. Interacting Multiple Model

Although the IMM is mostly used for tracking objects maneuvering with linear motion and objects in clutter [45], the approach is further tailored within the VSD filter for tracking CMS. The size of the process noise added while estimating unknown thrust states in a single VSD filter impacts the performance of the filter as the thrust size varies. For larger cases, the process noise helps prevent filter divergence, whereas the same level of noise for a smaller thrust results in an inability to accurately estimate the thrust. Because the thrust is assumed unknown a priori and during the maneuver, the IMM provides an advantage by combining the inputs of various filters that have different levels of process noise.

The IMM is a suboptimal hybrid estimation approach that uses a weighted combination of filter outputs to determine an estimate. The IMM is memoryless and dependent upon certain jump probabilities $\boldsymbol{Pr}_{j|k}$ at each time step. When using the IMM in tracking CMS, there is not a need to jump between varying noise models. Instead, it is more effective to use the formulation of the IMM and allow for residual-based weighting of all the models. Switching in an IMM occurs according to a heuristic-based jump probability matrix at each observation and decreases performance in this application. When using a Gaussian mixture of filters to track CMS, it is best to set the probabilities of switching between models to near zero and vary the process noise levels within the filters. Existing IMM methods call for maneuver verses nonmaneuver models combining at each step; however, this is very inefficient for spacecraft tracking because errors are quite large when using thrusting models to estimate a nonthrusting spacecraft. To use the IMM within the VSD paradigm, the IMM initiates after the maneuver is detected and terminates after the end of the maneuver. The IMM begins after covariance inflation, as discussed in Sec. III.B.

Adapting the IMM within the VSD filter after a maneuver is detected allows for several benefits. First, it does not limit the estimate to a single-process noise filter, which improves thrust estimates. Also, the weights determined by the IMM provide an initial solution for the best noise to use during postprocessing refinement. Similar to the EKF and UKF, the outputs of the IMM are improved via a fixed-lag-mode matching smoother [37,38]. The combined IMM filter/smoother algorithm is provided in Appendix B to detail the application of the IMM to the CMS tracking scenario. Section V demonstrates through scenarios the benefits of the IMM when compared to a single-model VSD approach.

IV. Simulation

To test the performance of the newly developed VSD EKF (Sec. III.B), a similar VSD UKF, and a VSD multiple-process noise IMM, a spacecraft is simulated in a 500 km noninclined circular orbit. Sixteen ground-based radars are equally spaced longitudinally and placed at a latitude of 5 deg. The purpose of this setup is to simulate constant coverage of the spacecraft. If the spacecraft is in view, each radar collects observations at 1 Hz, unless otherwise specified. Error is added to each observation with the following standard deviations: 1 m for range, 0.01 deg for azimuth and elevation, and 50 mm/s for range rate. The error factors simulate the observation noise present in a very accurate mechanical tracking radar. Increasing radar noise errors will increase true position errors and thrust estimation errors; however, it will not greatly impact the maneuver-detection results because the approaches are covariance based. In Sec. III.B, $\boldsymbol{R}$ is a diagonal matrix containing the appropriate variances for each observation, and $\boldsymbol{Q}$ during nonthrusting times is a matrix of zeros because only two body-assumptions are used.

After one complete orbit, the spacecraft maneuvers for 1500 s in the tangential direction with a thrust acceleration as detailed in Table 1. Then, the spacecraft is tracked for an entire orbit after maneuver completion. A maneuver is declared using limits on both Ψ

Table 1 Thrust acceleration in the velocity vector direction for simulated cases

Parameter	Case 1	Case 2	Case 3	Case 4	Case 5
th_a, mm/s^2	100	50	10	5	1

and Θ, and then the covariance is increased to an inflation threshold of 1. The maneuver is considered complete using the various methods discussed previously, and then the covariance is again increased to a threshold of 1 as outlined in Sec. III.B.

A smoother is run over filter data every 10 observations in the single and IMM formulations. The filter-smoother test in Eq. (12) is conducted at every observation. Data are smoothed every 10 observations as well when using the multiple-filter approach to determine the conclusion of the maneuver. Each of the five maneuvers is simulated 15 times using the same observation noise. Each run is different as added random noise is resampled each time. The UKF parameters are set to $\alpha_{\text{UKF}} = 0.1$, $\beta_{\text{UKF}} = 2$, and $\kappa_{\text{UKF}} = -3$ within the routine [25].

When using the multiple-model strategy from Sec. III.A to determine the conclusion of a maneuver, a nominal filter is run with the VSD output at 10 observation intervals after the start of the maneuver. Ψ and Θ are evaluated for 1000 s to determine if they exceed the thresholds of 30 and 4.5, respectively. Similar to the standard VSD approach, the covariance is inflated immediately after the transition until the trace of the covariance is larger than 1. After allowing 100 s for the filter to settle, the first case in which Ψ or Θ remain below the threshold for the entire 1000 s is selected as the best guess for the conclusion of the maneuver.

The single-model VSD and five model IMM values for $\boldsymbol{Q}_{\text{Add}}$ in the 1 Hz scenarios are detailed in Table 2. The values for the models were determined via sample testing of various diagonal noise vectors. The starting value for the initial weights in the IMM are $\boldsymbol{\mu} = [0.2 \quad 0.2 \quad 0.2 \quad 0.2 \quad 0.2]^T$. Additionally, the diagonals of the $\boldsymbol{Pr}_{j|k}$ matrix are set to 0.999999 with all off-diagonals set to $2.5 \cdot 10^{-7}$. These starting values ensure that each model has an equal opportunity of selection, and jumping between models is minimized within the IMM. Through mixing and likelihood weighting at each time step, the IMM determines the best model. For each level of thrust, the best $\boldsymbol{Q}_{\text{Add}}$ noise level is relatively constant; therefore, it is not necessary to jump between models at each time observation. Instead, the IMM approach is used to tune the filtering to account for various thrust sizes and process noise levels. The set of five models was determined during initial testing and deemed large enough to span the set of maneuver magnitudes simulated. Five models is also a small enough set to avoid degrading solution accuracy by averaging accurate and inaccurate model estimates. A pruning filter is another approach to model selection but is not considered in this paper because the traditional IMM was successful in converging on the maneuver solution. The IMM is only run after the maneuver is detected and concludes when the maneuver has ceased as determined by the methods discussed previously.

V. Results

Developing tracking approaches for a CMS requires special consideration of maneuver-detection approaches. The first section of the results, Sec. V.A, compares performance of the filter-smoother test and the maneuver-detection scalar Ψ in detecting the start of a maneuver. Section V.B compares the performance of four different methods to detect the end of the maneuver including the novel multiple-model approach. Section V.C compares the performance of the single adaptive VSD EKF and UKF models developed in Sec. III.B to an IMM tailored for spacecraft tracking as discussed in Sec. III.C. Next, comparisons are made by varying the frequency of observations. Finally, comments are provided for additional applications.

A. Maneuver Start Detection

Both the maneuver-detection scalar Ψ and filter-smoother consistency test Θ provide an accurate method to determine maneuvers; however, each has its advantages and disadvantages. Ψ requires tuning the limit to the orbit regime and observations. At times, large observation gaps or residuals cause a sharp increase in Ψ; therefore, for precise, small maneuver applications, it is necessary to evaluate past data to determine an appropriate maneuver threshold. Additionally, if a radar is prone to spurious measurements, a window of Ψ measurements are necessary to determine the difference between the start of a maneuver and a bad data point. The benefit of this method is that it works in real time with the filter, and a maneuver is detected during the processing of the observation. Θ is more robust because it is less susceptible to false-positives during large data gaps. The filter-smoother test requires running a smoother, which works backward in time. This feature requires the test to run on blocks of data; therefore, it is not real-time and is dependent on the frequency at which the smoother is run. The filter-smoother test can only detect maneuvers that occur within the window of the smoother. If the smoother timing is perfect, the maneuver in case 1 is detected exactly at the start. Figure 2 shows the test detecting the start of the maneuver when the smoother is begun 10 s after the maneuver. The vertical lines in the plot define the smoother intervals and the threshold detection is set to 4.5.

Using the same 10 s smoother window, if the start of the window is not perfectly timed, the detection of the start of the maneuver is estimated early in the smoothed block. Figure 3 shows how this affects when the maneuver is detected. Figures 2 and 3 show how well the filter-smoother test performs in detecting a maneuver but also how dependent the test is on the timing and length of the smoother window. The larger the smoother window is, the better the smoother averages the filter. Because the smoother runs after a batch of observations is collected, a larger window results in a larger delay in detecting a maneuver. This effect highlights a tradeoff in using the filter-smoother test. During testing when observations are collected at 1 Hz, a smoother window of 10 s is short enough to detect the maneuver quickly and large enough to improve filtered state estimates. Tuning the smoother window improves the filter-smoother test, and tuning depends on the observation frequency and any observation gaps.

The maneuver-detection scalar Ψ serves as a way to assess the error in an estimate without actually knowing the true location of the spacecraft as Ψ highlights any disparities between the covariance size and residual size. For these reasons, it proves effective in detecting maneuvers in real time without the need to work backward in time as the smoother does [25,27]. Figure 4 highlights a real-time version of the VSD filter using Ψ as a transition threshold. The figure shows how Ψ grows above the threshold quickly for case 1. At the next observation, the covariance is inflated, and the states are augmented to estimate the thrust. Figure 4 shows how the covariance inflation drops Ψ below the threshold and the thrust estimating keeps Ψ below the threshold until the conclusion of the maneuver.

Across all five cases, each simulated 15 times, Fig. 5 shows the performance of each method using tuned detection thresholds of 30 for Ψ and 4.5 for Θ. For the filter-smoother case, a fixed interval smoother is used after every 10 observations. The filter-smoother test is perfect at detecting the start of the maneuver for the two largest test

Table 2 Process noise configurations for the single-model VSD and IMM

Parameter	Single model	IMM model 1	IMM model 2	IMM model 3	IMM model 4	IMM model 5
$\boldsymbol{Q}_r$	10^{-9}	10^{-9}	10^{-10}	10^{-11}	10^{-12}	10^{-13}
$\boldsymbol{Q}_v$	10^{-12}	10^{-12}	10^{-13}	10^{-14}	10^{-15}	10^{-16}
$\boldsymbol{Q}_{\text{th}}$	10^{-12}	10^{-12}	10^{-13}	10^{-14}	10^{-15}	10^{-16}

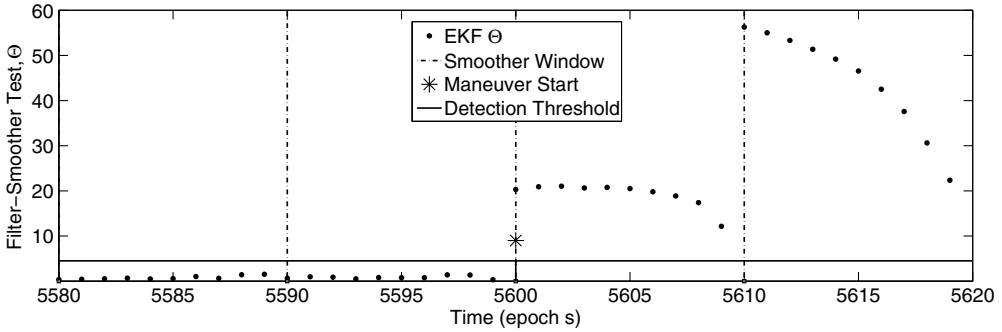

Fig. 2 Case 1 maneuver detection when smoother window is ideally timed.

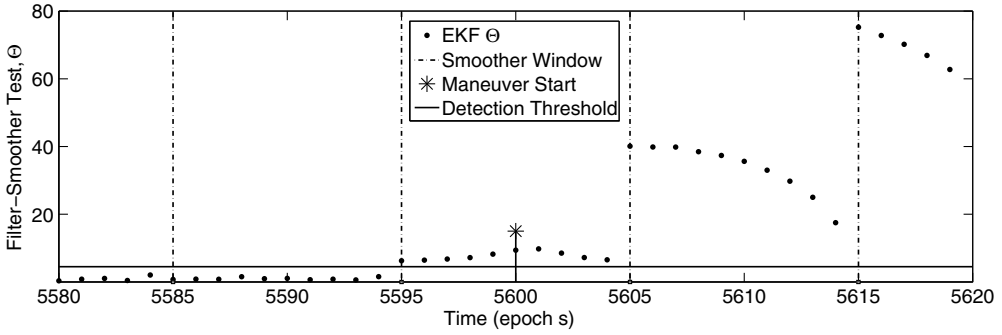

Fig. 3 Case 1 maneuver detection when smoother window is ill-timed.

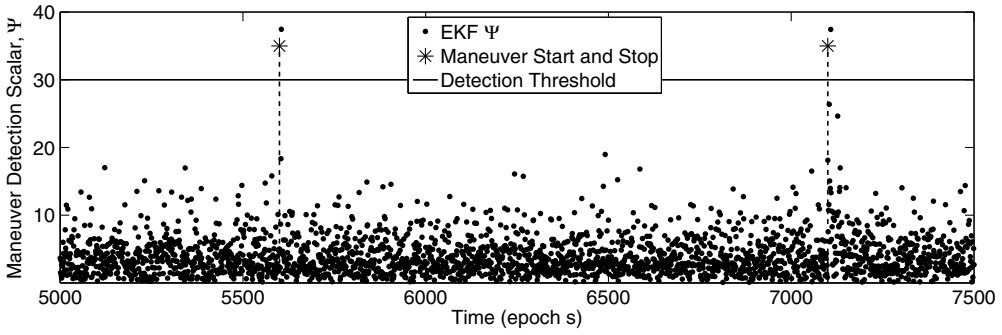

Fig. 4 Detecting maneuver start and conclusion with Ψ.

cases. This performance is linked to the fact that the smoother windows were aligned with the start of the maneuver, as in Fig. 2. Across all cases, the filter-smoother test outperforms Ψ, which shows the strength of the proposed approach as well as the benefit of using the smoother to improve filter estimates by working backward in time. The figure also shows that, as the thrust acceleration level decreases, both methods detect the start of the maneuver later and later. This trend results from the fact that the acceleration changes are so small that they are within the observation noise. As the spacecraft continues to thrust at a small acceleration, eventually the errors build up over time, and the maneuver is detected.

B. Maneuver End Detection

In Sec. III.A, the multiple-model approach to determine the end of a continuous maneuver was introduced to handle low-thrust cases when using a single VSD model. For larger-thrust cases, however, the same tests to detect the start of a maneuver can identify the conclusion of a maneuver. Figure 6 shows the filter-smoother test determining

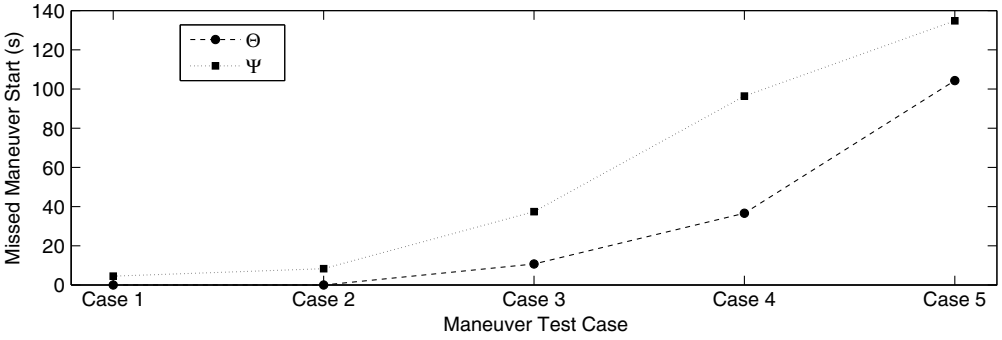

Fig. 5 Average error in detecting maneuver start for each case.

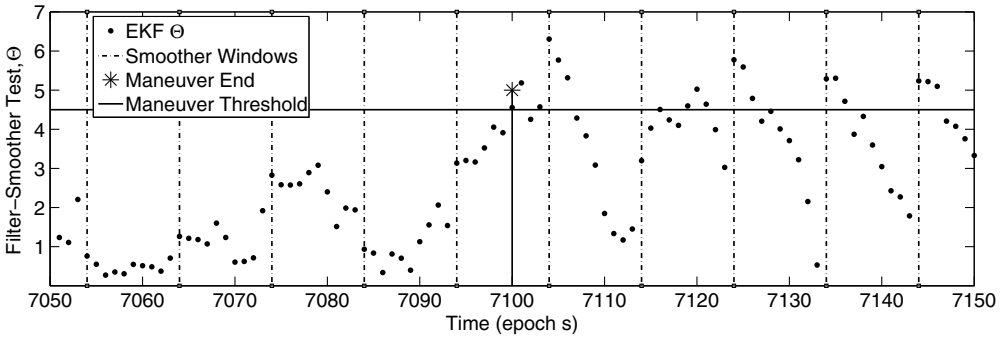

Fig. 6 Detecting maneuver end for case 1 using filter-smoother test.

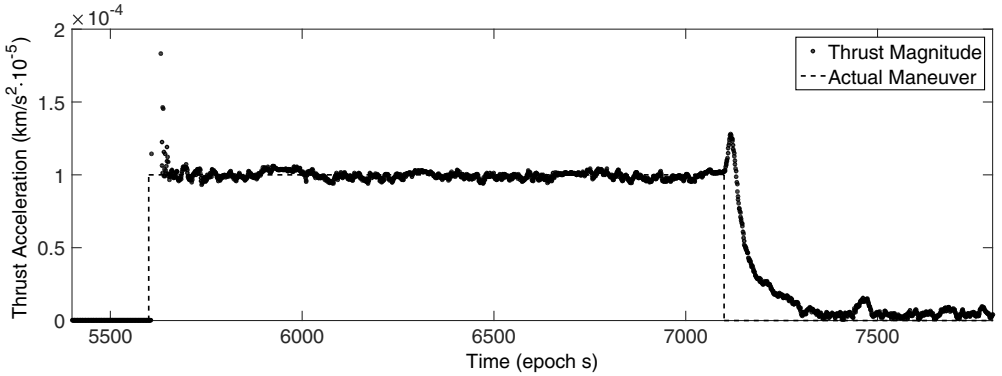

Fig. 7 Case 1 thrust magnitude estimate with single VSD filter.

the end of the maneuver for case 1 using a threshold of 4.5. The filter-smoother test detects the conclusion of the maneuver for all 15 runs of case 1 but only for four of the 15 runs of case 2. For Ψ, the end of the maneuver is more difficult to identify. Although Fig. 4 shows a single run where the end of the maneuver is detected, out of the 15 runs of case 1, Ψ signaled the end of the maneuver for only two of the runs.

Another way to detect the end of the maneuver, as discussed in Sec. III, is to simply evaluate the change in the estimated thrust magnitude $|\text{th}_a|_2$ to determine when the maneuver has ceased. Figure 7 shows how the end of the maneuver is detected by evaluating the magnitude of the thrust for one run of case 1. The dashed square wave is the actual thrust magnitude of the simulated spacecraft. This approach initially takes several observations for the filter to converge on the maneuver after the covariance inflation. If the covariance is not increased, near perfect knowledge is required for the start and magnitude of the maneuver to prevent filter divergence. Once the filter locks on the maneuver, it remains locked until the spacecraft concludes the maneuver. It takes the filter over 100 s to begin estimating the maneuver near zero. This approach detects the end of the maneuver in a simple way but is much slower than the filter-smoother test, as shown in Fig. 6. This method works in the exact same way for the single-model approach as it does within the IMM.

The results for detecting the end of case 1 using ψ_{th} [Eq. (17)] are captured in Fig. 8. The figure shows how this method calculates the end of the maneuver 30 s late, which is faster than the thrust magnitude method; however, the process still requires some tuning to declare maneuver completion. For both the thrust magnitude and ψ_{th} approaches, the tuning method is not exact. By looking at the curves shown in Figs. 7 and 8, a visual inspection shows the end of the maneuver, but only after levels reach consistent near-zero values. Figure 8 shows a sinusoidal pattern for ψ_{th} which is a result of the interaction between the inertial frame thrust coordinates, the thrust acceleration in the velocity direction, and the associated covariances. If the maneuver is in some combination of the radial, velocity vector, and normal directions, the shape of ψ_{th} changes, but a pattern is still easily recognizable. The pattern allows for slightly faster detection of the conclusion of the maneuver when compared to the thrust magnitude approach because once the sine wave breaks pattern, the conclusion of the thrust is realized. Additionally, this method is directly portable to the IMM approach because it relies only on the estimate thrust state and covariance.

Continuous-thrust maneuvers are more difficult to detect than a large, near-instantaneous maneuver due to the small size of continuous-thrust accelerations. The conclusion of the maneuver is more difficult to determine than the start of the maneuver because the filter has a less accurate orbit fit while the maneuver is occurring. This decreased accuracy is directly related to the fact that the thrust acceleration is unobservable. Table 3 shows the application of each

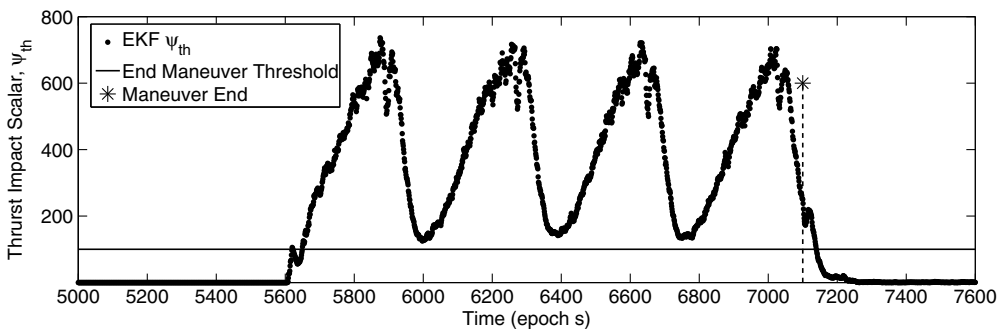

Fig. 8 Maneuver end detection using single-model ψ_{th}.

Table 3 Errors in determining maneuver end

	Case 1		Case 2		Case 3		Case 4		Case 5	
Parameter	Limit	Miss, s	Limit	Miss, s	Limit	Miss, s	Limit	Miss, s	Limit	Miss, s
Ψ	30	13.5	30	15.7	30	41.3	30	65.5	30	117.2
Θ	4.5	2.5[a]	4.5	11	4.5	23.3	4.5	33.5	4.5	105.2
ψ_{th}	125	27.8	25	35	0.15	93.4	— —	— —	— —	— —
$\text{IMM}_{\psi_{\text{th}}}$	125	31	200	10.7	50	62.2	2.0	91.5	0.25	360.5
$\lvert\text{th}_a\rvert_2$	$5 \cdot 10^{-5}$	60.4	$2.5 \cdot 10^{-5}$	58.6	$2.5 \cdot 10^{-6}$	114.5	— —	— —	— —	— —
$\text{IMM}_{\lvert\text{th}_a\rvert_2}$	$5 \cdot 10^{-5}$	54.3	$2.5 \cdot 10^{-5}$	55.7	$5 \cdot 10^{-6}$	73.9	$2.5 \cdot 10^{-6}$	86.9	$5 \cdot 10^{-7}$	179.7

[a]Using single-model threshold.

method in determining the average stop time for 15 runs of each maneuver case. The table shows that, as the maneuver gets smaller, the task of estimating the end of the maneuver becomes much more difficult, especially for the single-model approaches. For all cases, an EKF is used; and for the IMM, only the $|\text{th}_a|_2$ and ψ_{th} method results are listed. For the filter-smoother test, a fixed interval smoother is used after every 10 observations. For Ψ and Θ, a new nominal filter is begun after every 10 s, and the first to remain under the threshold is selected as the best estimate.

As discussed previously, the Θ and Ψ approaches for detecting the end of the maneuver are quick to determine the end of the thrust but only reliable for large maneuvers. The threshold approach using Θ was reliable and effective for only case 1, whereas the Ψ threshold was not reliable for any maneuver type once all 15 runs were considered. When small-magnitude thrusting stops, the thrust level is too low to generate a large enough error to exceed the stop maneuver threshold; therefore, a multiple-model strategy is necessary. Table 3 summarizes the results of the novel multiple-model approach to determine the end of the lower-acceleration continuous-thrust test cases using the output from the single-process noise VSD model. Based on the multiple-model strategy of selecting the first case in which Θ and Ψ remained within limits, all results predict the maneuver ending before the actual end of the maneuver. This result is an artifact of the strategy and is expected. Just as the methods take longer to detect smaller maneuvers, the multiple-model strategy assumes a good fit before the end of the maneuver because the thrust is too small to deviate the orbit fit. The multiple-model strategy provides a more accurate initial estimate of the maneuver conclusion compared to ψ_{th} and $|\text{th}_a|_2$ approaches. The method provides a way to determine the end of the smallest thrust acceleration when all other single VSD model methods fail. The multiple-model approach to determine the end of the thrust can handle IMM outputs but was not considered due to the similarities with the single-model approach. The only difference is that the multiple-model end thrust approach would use the state estimate from the IMM instead of from the single-process noise model.

The single-model ψ_{th} method is able to determine the conclusion of the thrust for the three larger maneuver cases. The level of the maneuver conclusion threshold varies for different size maneuvers. The sinusoidal wave seen in Fig. 8 shifts lower or higher depending on the size of the maneuver and size of the process noise added. A visual inspection of the curve provides a good choice for the threshold. The different selected thresholds are shown in Table 3 for the 15 cases run for both the IMM and single model. Also, the table shows that ψ_{th} outperforms the thrust magnitude approach in determining the end of the maneuver for the larger cases. This trend reveals that the inclusion of the inverse covariance (information matrix) aides in detecting the end of the maneuver. Once the thrust acceleration decreases to 5 mm/s^2, the sinusoidal curve seen in Fig. 8 becomes much less observable for the single-model case and the end of the thrust is indeterminable. When using the IMM, the process noise of several models are mixed, and the method can detect the end of every thrust simulation. The smaller the thrust is, the less likely the $\text{IMM}_{\psi_{\text{th}}}$ method is to outperform the $\text{IMM}_{|\text{th}_a|_2}$ approach.

Table 3 shows that the thrust magnitude for the single model is able to determine the conclusion of the larger thrusts. Figure 9 shows the difference between estimating the end of the thrust using $|\text{th}_a|_2$ and $\text{IMM}_{|\text{th}_a|_2}$ for case 5. The figure shows that the single-model thrust magnitude estimate is far from the truth and does not change when the maneuver ends. The IMM approach favors a small amount of process noise for small thrusts and is able to accurately estimate the maneuver and its conclusion. Figure 9 reveals the benefits of combining the IMM within the VSD for cases when the general order of magnitude of the thrust is unknown. All estimates of the conclusion of the thrust using the thrust magnitude method occur after the actual thrust conclusion. Additionally, it is important to highlight that, even though the single-model approach poorly models the thrust, the multiple-model approach to determine the maneuver conclusion still outperforms $\text{IMM}_{|\text{th}_a|_2}$.

From the five different maneuver cases each with 15 runs, the filter-smoother approach proved most successful at determining the beginning and end of the maneuvers. Additionally, if the orbit estimation routine is tied directly to the radar and required to run in real time, then the Ψ multiple-model approach was next best in determining the beginning and end of the maneuver. Finally, the IMM approach is able to modify the level of process noise to accurately model lower thrusts.

C. Error Analysis

The simulation results show the ability of the filter to detect the maneuver, adapt dimensions, estimate the thrust acceleration, and detect the end of the maneuver. One method to evaluate the perfor-

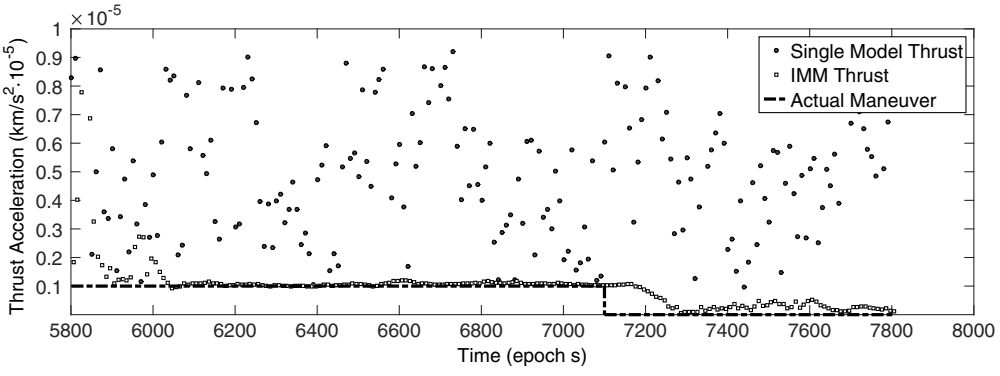

Fig. 9 Case 5 thrust magnitude estimates using a single model and IMM.

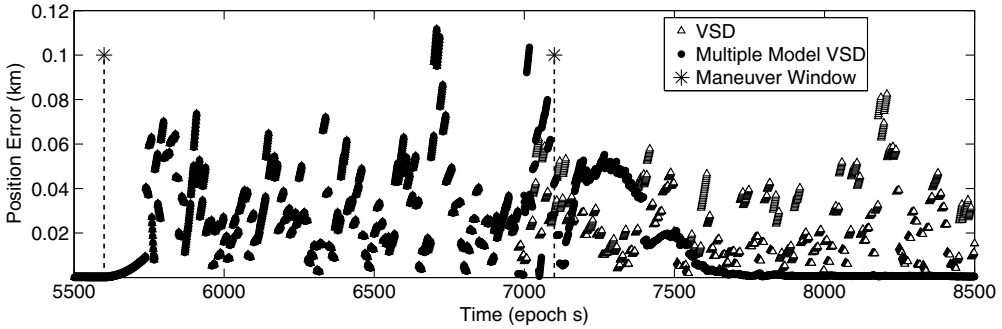

Fig. 10 Position error using multiple-model maneuver end detection for case 5.

mance of the algorithms is to determine the rms error between the truth orbit and the smoother estimated orbit during the maneuver:

$$\mathrm{RMS}_r = \sum_{i}^{N} |\boldsymbol{r}_{\mathrm{true}_i} - \boldsymbol{r}_{\mathrm{est}_i}|_2 \tag{36}$$

Another metric to evaluate and assess the VSD single model and IMM approaches is to determine the percent error of the thrust estimate while the maneuver is occurring:

$$\Delta v_{\mathrm{err}} = \sum_{i}^{N} \frac{||\mathrm{th}_{a_i}^{\mathrm{true}}|_2 - |\mathrm{th}_{a_i}^{\mathrm{est}}|_2|_1}{|\mathrm{th}_{a_i}^{\mathrm{true}}|_2} \cdot 100 \tag{37}$$

There is much research effort placed on determining the start and stop of the maneuver because the orbital solution is much less accurate when estimating a thrust that is not occurring. Figure 10 shows the error differences that are incurred when inaccurately determining the end of the maneuver. Comparing the multiple-model thrust end determination approach with the nominal single-model VSD, Fig. 10 displays the results of one of the 15 runs of case 5. Determining the approximate end of the maneuver greatly reduces the error. The summed error for every second for the time period displayed is 53.2 km for the multiple-model case and 74.9 km for the nominal VSD filter. Although the thrust is small, an inability to detect the end of the maneuver results in quickly building errors and a poor orbital solution. Without the multiple-model thrust end approach, the thrust is assumed to still occur, and errors continually build due to modeling a maneuver that is not occurring.

During analysis of the start and stop miss times shown in Fig. 5 and Table 3, both UKFs and EKFs were initially tested. The results were nearly identical; therefore, only the EKF was used to determine the full results in the tables due to its computational speed. The UKF is reintroduced to evaluate the errors once the start and stop times of the maneuvers are estimated using the EKF. To compare the performances of the EKF to the UKF, the estimated start and stop times of the maneuver for each test case resulting from the filter-smoother tests are used to run the single-model VSDs on simulated data. Additionally, the IMM approach using five models each with an EKF and different process noise as outlined in Sec. IV is run with identical start and stop times. The errors determined from the smoother estimates are summarized in Table 4.

The Δv_{err} error column in Table 4 captures the average error in estimating the magnitude of the maneuver after the filter has settled and before the end of the maneuver (epoch seconds 5800–7100). This magnitude percent error evaluates the steady-state performance of the additional state filters and the average percent error of the magnitude of the thrust estimated. The position error column is calculated using a span of observations from 100 s before the maneuver through 400 s postmaneuver (epoch seconds 5500–7500). The results pertain to an observation frequency of 1 Hz and are the average of 15 runs. The table shows how closely the EKF and UKF perform. Because the observation errors are normally distributed, it is anticipated that the filters will perform similarly. The filters are both designed and derived to minimize normally distributed errors. The linearization of the errors performed in the EKF did not compromise the results due to the frequency of observations. The UKF avoids the linearization while sacrificing computational time, taking about 10 times longer to run. For cases when radars collect observations often and at high frequencies with a high-fidelity propagator, the EKF is the better choice because it is faster, and errors are well approximated through lineartization. If radars are of poor quality and collecting data infrequently, and if a simple propagator is used, the UKF is the superior choice because it better handles unmodeled nonlinearities. The results also show that the single-process noise model VSD, using either the UKF or EKF, estimates the thrust magnitude very accurately for larger-thrust cases (Fig. 7) and poorly for the low-thrust cases (Fig. 9). This result is expected because a percent error metric allows for larger errors when the thrust magnitude is larger.

For the simulations tested, the larger the maneuver is, the more process noise is required to prevent filter divergence. The IMM evaluates five models at each time step and weights the model based on its residual likelihood, as shown in Appendix B. The weights of each model, $\boldsymbol{\mu}$, for each test case and all runs are summed and normalized in Fig. 11. As alluded to earlier, the weights clearly show that the IMM favors more process noise during larger maneuver scenarios and less during smaller maneuvers. This figure supports the results in Table 4. The single-model VSD EKF has a much larger $\boldsymbol{Q}$ than the weighted IMM; therefore, the EKF has larger errors for smaller-thrust cases.

Additionally, Fig. 11 shows for case 1 that the largest weighted input does not correspond to the largest noise. The single model has a consistent position noise of $\boldsymbol{Q}_r = 10^{-9}$ and lower overall error. Yet, the IMM better estimates the thrust and has larger position errors. The IMM, in a suboptimal way, selects the best weights at each observation in a memoryless fashion. Therefore, slightly growing errors over many observations are not realized, as opposed to a large error between two observations. Figure 12 shows how the IMM fails to add enough process noise to decrease errors as compared to a larger constant noise source. The results in Table 4 show the abilities of the IMM to accurately estimate thrusts at all levels. Overall, the IMM provides more flexibility to handle a wider range of thrusts; however, a properly tuned, single-model approach can provide better results.

Table 4 Thrust and position error comparison between cases and filters

	Case 1		Case 2		Case 3		Case 4		Case 5	
Filter	Δv_{err}, %	RMS_r, km	Δv_{err}	RMS_r, km	Δv_{err}	RMS_r, km	Δv_{err}	RMS_r, km	Δv_{err}	RMS_r, km
EKF	2.1	55.1	3.9	61.9	20.0	56.6	50	59.2	395.3	54.8
UKF	2.1	55.2	3.9	61.7	20.0	56.6	50	59.1	395.3	54.9
IMM	1.8	72.5	2.4	65.6	3.9	52.3	6.6	50.4	59.1	38.9

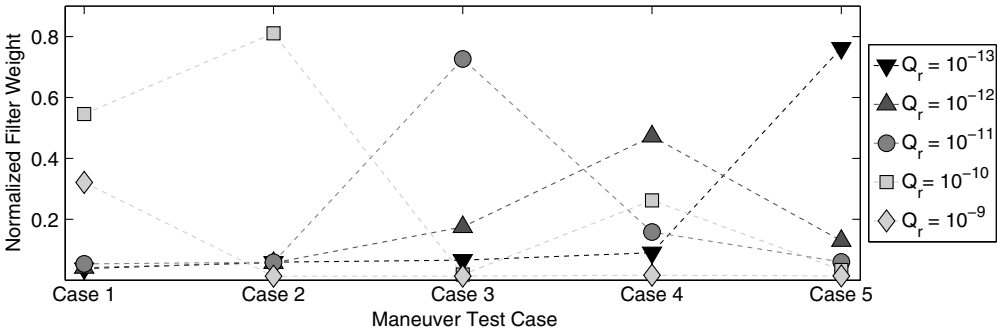

Fig. 11 VSD IMM normalized filter weights for each case.

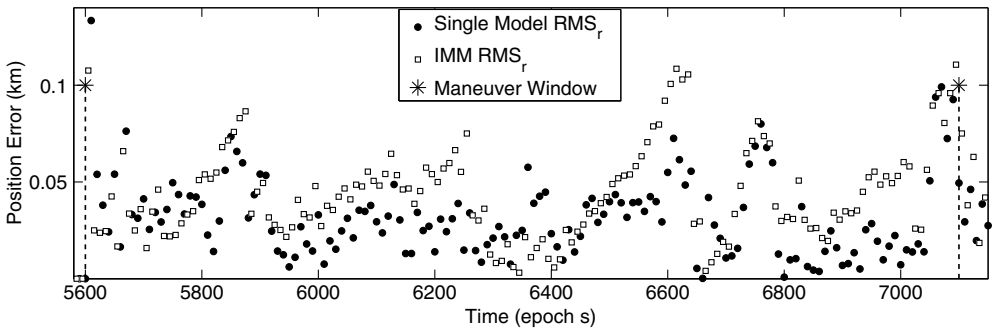

Fig. 12 Case 1 position errors for a single model compared to an IMM.

D. Observation Frequency

For high-priority, noncooperative orbit determination, it is critical to use as much data as possible to improve the orbit estimate. To illustrate the impact of using high-frequency observations, the single-model VSD case 5 is performed 15 times for several different observation frequencies. Each observation frequency required tuning the added process noise $\boldsymbol{Q}$. The values of $\boldsymbol{Q}$ are determined by scaling the noise based on the observation frequency to achieve an equal comparison among the different approaches.

Proceeding in a similar fashion as performed in previous sections, first the start and stop maneuver times are evaluated. Table 5 reveals that increasing the observation frequency does not correspond to a faster maneuver detection; in fact, it is slower. This result is a product of the KF routine and the very small thrust accelerations. With more frequent observations, the state is continually updated while averaging the errors associated with the undetected maneuver. With less frequent observations, the thrust accelerations cause larger errors resulting in an earlier maneuver detection. For each frequency, 10 observations are processed before running a smoother. Therefore, for the 0.1 frequency case, 1 s of observations is processed; 100 s of observations are processed before smoothing for the 10 s observation frequency case. The larger smoothing window allows the less-frequent observation approach to outperform the short frequency case in detecting the start of the maneuver. The short frequency case outperforms the less-frequent observation case when using the multiple-model approach in Fig. 1 at 10 observation intervals to detect the conclusion of the maneuver. Overall, adding more frequent observations does not improve the filter's ability to determine the start of the maneuver; however, the ability to determine the end of the maneuver using multiple models is improved when the time between observation decreases, as is evident when comparing Table 3–Table 5.

Next, the errors of each approach are compared in Table 6 using the results from Table 5. The position error is the magnitude error from the smoother for case 5 for a period of 2000 s that include the entire maneuver (epoch seconds 5500–7500). The error is determined by summing the rms position error every 10 s. Δv_{err} is the average percent error from epoch seconds 5800–7100, which is the time after the filter settles until the end of the thrust. The results for the position error for case 5 are not exactly 1/10th of the error displayed in Table 4 due to the fact that the error is not evenly distributed and points were selected every 10 s. Increasing the observation frequency was not intended to improve the Δv estimation as was accomplished with the IMM; instead, the results compare the position error impact of increasing the observation frequency. The error decreases significantly as the observations increase. The higher-frequency 10 Hz (0.1 s) case outperforms the 1 Hz case for nearly the entire period of the thrust estimation. The results in Table 6 solidify the proposal that increasing the observation frequency from the same radar improves the tracking solution when all other variables are held constant. Therefore, when available, it is best to use as much of the data as possible from the radar to track the noncooperative spacecraft.

E. Additional Applications

The simulations tested all provided constant coverage of the CMS, which is not likely in operational tracking. The scenarios were purposefully designed to test the abilities of the VSD and IMM approaches in a simple environment. Because of limited ground site resources and observation geometry, a realistic orbit determination routine for a high-priority spacecraft will contain coverage gaps because sensors are sparse. The novel multiple-model approach

Table 5 Maneuver detection for case 5 with varying observation frequencies

Observation frequency, s	Method	Limit	Start miss, s	Stop miss, s
10	Ψ	30	143	215.7
10	Θ	4.5	91	174.3
0.1	Ψ	30	123.2	94.1
0.1	Θ	5	104.7	81.5

Table 6 Position and thrust error when observation frequency is varied

Observation frequency, s	$\boldsymbol{Q}_p$	$\boldsymbol{Q}_v$ and $\boldsymbol{Q}_{\text{th}}$	Δv_{err}, %	RMS_r
10	10^{-8}	10^{-11}	393	8.3
1	10^{-9}	10^{-12}	390	5.3
0.1	10^{-10}	10^{-13}	326	3.0

developed and tested can also serve as a way to handle coverage gaps. If the spacecraft is maneuvering as it exits coverage, the multiple-model approach can use a baseline model that assumes the thrust continues and then use other models to estimate the end of the thrust at different intervals. This approach provides a set of possible thrust durations and locations of the spacecraft. Once the radar reacquires the spacecraft, the closest of the multiple models is selected as the best guess for the thrust that occurred outside of view. This topic is planned for additional research in future efforts and undoubtedly necessary for the transition of the developed methods for operational use.

Additionally, the VSD and IMM can process data from observations made by any sensor, as long as the observation errors are understood. Both methods are directly portable to higher-fidelity orbit propagators and estimation routines. Once the maneuver is estimated via the smoother, some assumptions may improve the solution quality. If it is assumed that the maneuver is constant over the time window, the filter-smoother combination can reprocess the data while assuming a constant thrust. Also during postprocessing, different optimization and input estimation routines are implementable to further reduce errors now that the VSD approach detected start times, stop times, an initial estimate of the maneuver, and an IMM provided process noise estimate.

VI. Conclusions

Overall, the newly developed variable-state dimension (VSD) interacting multiple-model (IMM) algorithm is successful at performing orbit determination on a continuously maneuvering spacecraft (CMS), and the novel maneuver end multiple-model method provides accurate estimates of maneuver end times. Where traditional IOD and batch least-squares (BLS) methods fail to converge on an orbit, the VSD IMM with covariance inflation provides a new approach to perform tracking and orbit determination in real time for high-priority cases. In a congested and contested space environment, there is increased interest on fast and accurate space situational awareness (SSA) knowledge. Equipping orbit determination routines with the ability to detect maneuvers and transition to track spacecraft thrust accelerations as they maneuver will improve the orbital solution in real time and help pass accurate state estimates to additional radars.

Although the IMM approach provides the flexibility to handle maneuvers of all magnitudes, a well-tuned single-model filter can outperform the multiple-model approach. The research shows that, if the magnitude of potential maneuvers is known, the best solution is to tune a single VSD model for tracking. If little intelligence is available on a spacecraft that can quickly throttle maneuvers, an IMM approach is recommended during initial real-time processing and tracking. The initial thrust and state estimates from the VSD models provide excellent starting values for further analysis using optimization and refinement tools during postprocessing.

An increase in the frequency of observations for tracking a CMS decreases the errors. The key takeaway of this analysis is to gather as much data as possible while the spacecraft is in view and maneuvering. For tracking high-priority CMS, it is necessary to quickly task available radars and process as much data as possible within the VSD filter routines.

Maneuvering spacecraft are most critical to track because unknown maneuvers may result in failing to locate the spacecraft at a future time or cross-tagging the observation to the incorrect satellite. An important step in the future of improving SSA is understanding which satellites have the potential to maneuver and equipping orbit determination routines with the abilities to track these spacecraft as they maneuver. The covariance inflation VSD IMM with maneuver start and end detection abilities is an implementable tool to help improve SSA of high-priority targets.

Appendix A: State to Observation

Statistical orbit determination (SOD) techniques are applied by converting the state estimate to an observation estimate $\hat{\boldsymbol{y}}$ [8]. Define a vector that combines range and range rate vectors and is applicable to both the south, east, zenith (SEZ) and Earth-centered Earth-fixed (ECEF) frames, $\tilde{\boldsymbol{\rho}}_{\text{SEZ}} = [\rho_S \quad \rho_E \quad \rho_Z \quad \dot{\rho}_S \quad \dot{\rho}_E \quad \dot{\rho}_Z]^T$. Also, define $\varpi = \boldsymbol{\rho}_{\text{SEZ}} \cdot \dot{\boldsymbol{\rho}}_{\text{SEZ}}$. The state is converted to an observation using a series of equations [8]

$$\begin{aligned}\hat{\boldsymbol{y}} &= G_{\tilde{\rho}_{\text{SEZ}}\to\hat{y}} G_{\tilde{\rho}_{\text{ECEF}}\to\tilde{\rho}_{\text{SEZ}}} G_{\boldsymbol{x}_{\text{ECEF}}\to\tilde{\rho}_{\text{ECEF}}} G_{\boldsymbol{x}_{\text{ECI}}\to\boldsymbol{x}_{\text{ECEF}}}(\boldsymbol{x}, t) \\ &= [\rho \quad \beta \quad \text{el} \quad \dot{\rho}]^T \end{aligned} \tag{A1}$$

$$G_{\boldsymbol{x}_{\text{ECI}}\to\boldsymbol{x}_{\text{ECEF}}} = \begin{bmatrix} \text{Rot}_{\text{ECI}\to\text{ECEF}} & 0 \\ \dot{\text{Rot}}_{\text{ECI}\to\text{ECEF}} & \text{Rot}_{\text{ECI}\to\text{ECEF}} \end{bmatrix} \tag{A2}$$

$$G_{\boldsymbol{x}_{\text{ECEF}}\to\tilde{\rho}_{\text{ECEF}}} = \begin{bmatrix} \boldsymbol{r}_{\text{sat,ECEF}} - \boldsymbol{r}_{\text{site,ECEF}} \\ \boldsymbol{v}_{\text{sat,ECEF}} \end{bmatrix} \tag{A3}$$

$$G_{\tilde{\rho}_{\text{ECEF}}\to\tilde{\rho}_{\text{SEZ}}} = \begin{bmatrix} \text{Rot}_{\text{ECEF}\to\text{SEZ}} & 0 \\ 0 & \text{Rot}_{\text{ECEF}\to\text{SEZ}} \end{bmatrix} \tag{A4}$$

$$G_{\tilde{\rho}_{\text{SEZ}}\to\hat{y}} = \begin{bmatrix} \sqrt{\rho_S^2 + \rho_E^2 + \rho_Z^2} \\ \tan^{-1}\left(\frac{-\rho_E}{\rho_S}\right) \\ \sin^{-1}\left(\frac{\rho_Z}{\rho}\right) \\ \frac{\varpi}{\rho} \end{bmatrix} \tag{A5}$$

Using Eq. (A1) to linearize the change by taking partial derivatives,

$$\boldsymbol{H} = \frac{\partial \boldsymbol{y}}{\partial \tilde{\boldsymbol{\rho}}_{\text{SEZ}}} \frac{\partial \tilde{\boldsymbol{\rho}}_{\text{SEZ}}}{\partial \tilde{\boldsymbol{\rho}}_{\text{ECEF}}} \frac{\partial \tilde{\boldsymbol{\rho}}_{\text{ECEF}}}{\partial \boldsymbol{x}_{\text{ECEF}}} \frac{\partial \boldsymbol{x}_{\text{ECEF}}}{\partial \boldsymbol{x}_{\text{ECI}}} \tag{A6}$$

$$\boldsymbol{H} = \frac{\partial \boldsymbol{y}}{\partial \tilde{\boldsymbol{\rho}}_{\text{SEZ}}} \begin{bmatrix} \text{Rot}_{\text{ECEF}\to\text{SEZ}}\text{Rot}_{\text{ECI}\to\text{ECEF}} & 0 \\ \text{Rot}_{\text{ECEF}\to\text{SEZ}}\dot{\text{Rot}}_{\text{ECI}\to\text{ECEF}} & \text{Rot}_{\text{ECEF}\to\text{SEZ}}\text{Rot}_{\text{ECI}\to\text{ECEF}} \end{bmatrix} \tag{A7}$$

$\partial \boldsymbol{y}/\partial \tilde{\boldsymbol{\rho}}_{\text{SEZ}}$ is a 4×6 matrix:

$$\frac{\partial \boldsymbol{y}}{\partial \tilde{\boldsymbol{\rho}}_{\text{SEZ}}} = [\boldsymbol{\Upsilon} \quad \boldsymbol{\Omega}] \tag{A8}$$

$$\boldsymbol{\Upsilon} = \begin{bmatrix} \frac{\rho_S}{\rho} & \frac{\rho_E}{\rho} & \frac{\rho_Z}{\rho} \\ \frac{\rho_E}{\rho_E^2+\rho_S^2} & \frac{-\rho_S}{\rho_E^2+\rho_S^2} & 0 \\ -\frac{\rho_S\rho_Z}{\rho^2\sqrt{\rho^2-\rho_Z^2}} & -\frac{\rho_E\rho_Z}{\rho^2\sqrt{\rho^2-\rho_Z^2}} & \frac{\sqrt{\rho^2-\rho_Z^2}}{\rho^2} \\ \frac{\dot{\rho}_S}{\rho} - \frac{\rho_S\varpi}{\rho^3} & \frac{\dot{\rho}_E}{\rho} - \frac{\rho_E\varpi}{\rho^3} & \frac{\dot{\rho}_Z}{\rho} - \frac{\rho_Z\varpi}{\rho^3} \end{bmatrix} \tag{A9}$$

$$\boldsymbol{\Omega} = \begin{bmatrix} 0 & 0 & 0 \\ 0 & 0 & 0 \\ 0 & 0 & 0 \\ \frac{\rho_S}{\rho} & \frac{\rho_E}{\rho} & \frac{\rho_Z}{\rho} \end{bmatrix} \tag{A10}$$

Appendix B: Interacting Multiple Model with Smoother

The IMM begins by defining r total models at time $t_i = t_0$. Each k model has an initial probability $\boldsymbol{\mu}_i^k$, initial state $\hat{\boldsymbol{x}}_i^k$, and covariance $\hat{\boldsymbol{P}}_i^k$. Additionally, define a square matrix $\boldsymbol{Pr}_{j|k}$ to contain the memoryless static mixing probabilities of transition from model j to k at each time step. Determine the initial mixing probabilities at the time of the next observation t_i using two steps. First, sum model probabilities for each model k up to a total of r models:

$$\bar{\boldsymbol{c}}_k = \sum_{j=1}^{r} \boldsymbol{Pr}_{j|k} \boldsymbol{\mu}_{i-1}^j \tag{B1}$$

Next, determine the mixing probabilities matrix:

$$\boldsymbol{\mu}_{i-1}^{j|k} = \frac{1}{\bar{\boldsymbol{c}}_k} \boldsymbol{Pr}_{j|k} \boldsymbol{\mu}_{i-1}^j \tag{B2}$$

for all r^2 model combinations. Then, determine the mixed state and covariance for each model k to r total:

$$\tilde{\boldsymbol{x}}_{i-1}^k = \sum_{j=1}^{r} \hat{\boldsymbol{x}}_{i-1}^j \boldsymbol{\mu}_{i-1}^{j|k} \tag{B3}$$

$$\tilde{\boldsymbol{P}}_{i-1}^k = \sum_{j=1}^{r} \boldsymbol{\mu}_{i-1}^{j|k} \{\hat{\boldsymbol{P}}_{i-1}^j + [\hat{\boldsymbol{x}}_{i-1}^j - \tilde{\boldsymbol{x}}_{i-1}^k][\hat{\boldsymbol{x}}_{i-1}^j - \tilde{\boldsymbol{x}}_{i-1}^k]^T\} \tag{B4}$$

Input $\tilde{\boldsymbol{x}}_{i-1}^k$ and $\tilde{\boldsymbol{P}}_{i-1}^k$ into filter k. Propagate and update each estimated state, covariance, residual, and residual covariance: $\hat{\boldsymbol{x}}_i^k$, $\hat{\boldsymbol{P}}_i^k$, $\boldsymbol{\nu}_i^k$, and $\boldsymbol{S}_i^k$. After running each model's filter, update the modal probability for each model via the likelihood function $\boldsymbol{\Lambda}_i^k \sim \mathcal{N}(\boldsymbol{\nu}_i^k; 0, \boldsymbol{S}_i^k)$:

$$\boldsymbol{\Lambda}_i^k = \frac{1}{\sqrt{|(2\pi)\boldsymbol{S}_i^k|}} e^{-\frac{1}{2}(\boldsymbol{\nu}_i^k)^T (\boldsymbol{S}_i^k)^{-1} \boldsymbol{\nu}_i^k} \tag{B5}$$

$$\boldsymbol{\mu}_i^k = \frac{\Lambda_i^k \bar{\boldsymbol{c}}_k}{\sum_{j=1}^{r} \Lambda_i^j \bar{\boldsymbol{c}}_j} \tag{B6}$$

where $|\boldsymbol{S}_i^k|$ is the determinant of $\boldsymbol{S}$. Combine all models for an overall IMM estimate:

$$\underline{\boldsymbol{x}}_i = \sum_{k=1}^{r} \hat{\boldsymbol{x}}_i^k \boldsymbol{\mu}_i^k \tag{B7}$$

$$\underline{\boldsymbol{P}}_i = \sum_{k=1}^{r} \boldsymbol{\mu}_i^k \{\hat{\boldsymbol{P}}_i^k + (\hat{\boldsymbol{x}}_i^k - \underline{\boldsymbol{x}}_i)(\hat{\boldsymbol{x}}_i^k - \underline{\boldsymbol{x}}_i)^T\} \tag{B8}$$

After processing all observations in an interval, estimates are improved with a smoother. Set $i = N$ at $t_i = t_N$, where N is the last observation of the smoothing interval. For all k models, set $\hat{\boldsymbol{P}}_N^{s^k} = \hat{\boldsymbol{P}}_N^k$, $\underline{\boldsymbol{P}}_N^s = \underline{\boldsymbol{P}}_N$, $\hat{\boldsymbol{x}}_N^{s^k} = \hat{\boldsymbol{x}}_N^k$, $\underline{\boldsymbol{x}}_N^s = \underline{\boldsymbol{x}}_N$, $\boldsymbol{\mu}_N^{s^k} = \boldsymbol{\mu}_N^k$. All smoother values contain the exponent s. Next, calculate backward transition probabilities:

$$\bar{\boldsymbol{e}}_k = \sum_{j=1}^{r} \boldsymbol{Pr}_{j|k} \boldsymbol{\mu}_{i-1}^j \tag{B9}$$

$$\boldsymbol{B}_{j|k} = \frac{1}{\bar{\boldsymbol{e}}_k} \boldsymbol{Pr}_{j|k} \boldsymbol{\mu}_{i-1}^j \tag{B10}$$

$$\bar{\boldsymbol{d}}_k = \sum_{j=1}^{r} \boldsymbol{B}_{j|k} \boldsymbol{\mu}_i^{s^j} \tag{B11}$$

$$\boldsymbol{\mu}_i^{s^{j|k}} = \frac{1}{\bar{\boldsymbol{d}}_j} \boldsymbol{B}_{j|k} \boldsymbol{\mu}_i^{s^j} \tag{B12}$$

where Eqs. (B9) and (B11) are defined for each model k up to r total, and Eqs. (B10) and (B12) are defined for all r^2 possibilities. Then, calculate the mode-matched mixed smoothing using:

$$\tilde{\boldsymbol{x}}_i^{s^k} = \sum_{j=1}^{r} \hat{\boldsymbol{x}}_i^{s^j} \boldsymbol{\mu}_i^{s^{j|k}} \tag{B13}$$

$$\tilde{\boldsymbol{P}}_i^{s^k} = \sum_{j=1}^{r} \boldsymbol{\mu}_i^{s^{j|k}} \{\hat{\boldsymbol{P}}_i^{s^j} + [\hat{\boldsymbol{x}}_i^{s^j} - \tilde{\boldsymbol{x}}_i^{s^k}][\hat{\boldsymbol{x}}_i^{s^j} - \tilde{\boldsymbol{x}}_i^{s^k}]^T\} \tag{B14}$$

$$\boldsymbol{A}_{i-1}^k = \hat{\boldsymbol{P}}_{i-1}^k \boldsymbol{\Phi}_i^{k^T} (\bar{\boldsymbol{P}}_i^k)^{-1} \tag{B15}$$

$$\hat{\boldsymbol{x}}_{i-1}^{s^k} = \hat{\boldsymbol{x}}_{i-1}^k + \boldsymbol{A}_{i-1}^k (\tilde{\boldsymbol{x}}_i^{s^k} - \bar{\boldsymbol{x}}_i^k) \tag{B16}$$

$$\hat{\boldsymbol{P}}_{i-1}^{s^k} = \hat{\boldsymbol{P}}_{i-1}^k - \boldsymbol{A}_{i-1}^k (\tilde{\boldsymbol{P}}_i^{s^k} - \bar{\boldsymbol{P}}_i^k)(\boldsymbol{A}_{i-1}^k)^T \tag{B17}$$

Subsequently, find the smoothed mode probability:

$$\boldsymbol{\Lambda}_{i-1}^k = \sum_{j=1}^{r} \boldsymbol{Pr}_{j|k} (\mathcal{N}(\hat{\boldsymbol{x}}_i^{s^j}; \bar{\boldsymbol{x}}_i^j, \bar{\boldsymbol{P}}_i^j)) \tag{B18}$$

$$\boldsymbol{\mu}_{i-1}^{s^k} = \frac{\boldsymbol{\Lambda}_{i-1}^k \boldsymbol{\mu}_{i-1}^k}{\sum_{j=1}^{r} \boldsymbol{\Lambda}_{i-1}^j \boldsymbol{\mu}_{i-1}^j} \tag{B19}$$

Finally, determine the IMM smoothed state and covariance:

$$\underline{\boldsymbol{x}}_{i-1}^s = \sum_{k=1}^{r} \hat{\boldsymbol{x}}_{i-1}^{s^k} \boldsymbol{\mu}_{i-1}^{s^k} \tag{B20}$$

$$\underline{\boldsymbol{P}}_{i-1}^s = \sum_{k=1}^{r} \boldsymbol{\mu}_{i-1}^{s^k} \{\hat{\boldsymbol{P}}_{i-1}^{s^k} + (\hat{\boldsymbol{x}}_{i-1}^{s^k} - \underline{\boldsymbol{x}}_{i-1}^s)(\hat{\boldsymbol{x}}_{i-1}^{s^k} - \underline{\boldsymbol{x}}_{i-1}^s)^T\} \tag{B21}$$

Continue smoothing until $t_{i-1} = t_0$ and the beginning of the smoothing interval is reached.

Acknowledgments

Special thanks to Brendan Houlton at Analytical Graphics, Inc., for recommending that the authors consider the filter-smoother test for detecting noncooperative maneuvers.

References

[1] "National Security Space Strategy Unclassified Summary," U.S. Dept. of Defense, Arlington, VA, 2011.

[2] National Research Council, *Continuing Kepler's Quest: Assessing Air Force Space Command's Astrodynamics Standards*, The National Academies Press, Washington, D.C., 2012, pp. 38–39, http://www.nap.edu/catalog/13456/continuing-keplers-quest-assessing-air-force-space-commands-astrodynamics-standards [retrieved 1 Oct. 2012].

[3] Baird, M. A., "Maintaining Space Situational Awareness and Taking It to the Next Level," *Air and Space Power Journal*, Vol. 27, No. 5, Sept.–Oct. 2013, pp. 50–73.

[4] Hough, M. E., "Recursive Bias Estimation and Orbit Determination," *Journal of Guidance, Control, and Dynamics*, Vol. 32, No. 2, 2009, pp. 645–653. doi:10.2514/1.39955

[5] Hough, M. E., "Orbit Determination with Improved Covariance Fidelity, Including Sensor Measurement Biases," *Journal of Guidance, Control, and Dynamics*, Vol. 34, No. 3, 2011, pp. 903–911. doi:10.2514/1.53053

[6] Wiesel, W. E., *Modern Orbit Determination*, Aphelion Press, Beavercreek, OH, 2003, pp. 93–104.

[7] Schutz, B., Tapley, B., and Born, G. H., *Statistical Orbit Determination*, Elsevier, Burlington, MA, 2004, pp. 159–213.

[8] Vallado, D. A., *Fundamentals of Astrodynamics and Applications*, 3rd ed., Springer, New York, 2007, pp. 105, 164, 165, 269, 459, 766–806.

[9] Vishwajeet, K., Singla, K., and Jah, M., "Nonlinear Uncertainty Propagation for Perturbed Two-Body Orbits," *Journal of Guidance, Control, and Dynamics*, Vol. 37, No. 5, 2014, pp. 1415–1425. doi:10.2514/1.G000472

[10] Hecker, M., "Expert System for Processing Uncorrelated Satellite Tracks," *Journal of Guidance, Control, and Dynamics*, Vol. 18, No. 5, 1995, pp. 1139–1144. doi:10.2514/3.21516

[11] Hujsak, R., "Orbit Determination During High Thrust and Low Thrust Maneuvers," *15th AAS/AIAA Space Flight Mechanics Conference*, American Astronautical Soc. Paper 2005-136, Springfield, VA, Jan. 2005.

[12] Wright, J. R., "Sequential Orbit Determination with Auto-Correlated Gravity Modeling Errors," *Journal of Guidance, Control, and Dynamics*, Vol. 4, No. 3, 1981, pp. 304–309. doi:10.2514/3.56083

[13] Wright, J. R., "Nonlinear Variable Lag Smoother," *18th AAS/AIAA Space Flight Mechanics Meeting*, American Astronautical Soc. Paper 303, Springfield, VA, Jan. 2008.

[14] Wright, J. R., Woodburn, J., Truong, S., and Chuba, W., "Orbit Gravity Error Covariance," *18th AAS/AIAA Space Flight Mechanics Meeting*, American Astronautical Soc. Paper 2008-157, Springfield, VA, Jan. 2008.

[15] Melvin, P. J., "A Kalman Filter for Orbit Determination with Applications to GPS and Stellar Navigation," *6th AAS/AIAA Spaceflight Mechanics Meeting*, American Astronautical Soc. Paper 1996-145, Springfield, VA, Feb. 1996.

[16] Julier, S. J., and Uhlmann, J. K., "Reduced Sigma Point Filters for the Propagation of Means and Covariances Through Nonlinear Transformations," *Proceedings of the American Control Conference*, Vol. 2, IEEE Publ., Piscataway, NJ, 2002, pp. 887–892. doi:10.1109/ACC.2002.1023128

[17] Julier, S. J., and Uhlmann, J. K., "Unscented Filtering and Nonlinear Estimation," *Proceedings of the IEEE*, Vol. 92, No. 3, 2004, pp. 401–422. doi:10.1109/JPROC.2003.823141

[18] Teixeira, B. O., Santillo, M. A., Erwin, R. S., and Bernstein, D. S., "Spacecraft Tracking Using Sampled-Data Kalman Filters," *IEEE Control Systems*, Vol. 28, No. 4, 2008, pp. 78–94. doi:10.1109/MCS.2008.923231

[19] Lee, D.-J., and Alfriend, K. T., "Sigma Point Filtering for Sequential Orbit Estimation and Prediction," *Journal of Spacecraft and Rockets*, Vol. 44, No. 2, 2007, pp. 388–398. doi:10.2514/1.20702

[20] Särkkä, S., "Continuous-Time and Continuous-Discrete-Time Unscented Rauch–Tung–Striebel Smoothers," *Signal Processing*, Vol. 90, No. 1, 2010, pp. 225–235. doi:10.1016/j.sigpro.2009.06.012

[21] Särkkä, S., "Unscented Rauch–Tung–Striebel Smoother," *IEEE Transactions on Automatic Control*, Vol. 53, No. 3, 2008, pp. 845–849. doi:10.1109/TAC.2008.919531

[22] Gelb, A., *Applied Optimal Estimation*, MIT Press, Cambridge, MA, 1974, pp. 285–288.

[23] Sorenson, H., and Sacks, J., "Recursive Fading Memory Filtering," *Information Sciences*, Vol. 3, No. 2, 1971, pp. 101–119. doi:10.1016/S0020-0255(71)80001-4-0255(73)90003-0

[24] Lee, T., "Theory and Application of Adaptive Fading Memory Kalman Filters," *IEEE Transactions on Circuits and Systems*, Vol. 35, No. 4, 1988, pp. 474–477. doi:10.1109/31.1769

[25] Goff, G. M., Showalter, D., Black, J. T., and Beck, J. A., "Parameter Requirements for Non-Cooperative Satellite Maneuver Reconstruction Using Adaptive Filters," *AIAA/AAS Astrodynamics Specialist Conference*, American Astronautical Soc. Paper 2014-4169, Springfield, VA, Aug. 2014.

[26] Bar-Shalom, Y., and Birmiwal, K., "Variable Dimension Filter for Maneuvering Target Tracking," *IEEE Transactions on Aerospace and Electronic Systems*, Vol. 18, No. 5, 1982, pp. 621–629. doi:10.1109/TAES.1982.309274

[27] Bar-Shalom, Y., Li, X. R., and Kirubarajan, T., *Estimation with Applications to Tracking and Navigation: Theory Algorithms and Software*, Wiley, New York, 2004, Chap. 11.

[28] Ramachandra, K., *Kalman Filtering Techniques for Radar Tracking*, CRC Press, Boca Raton, FL, 2000, Chap. 9.

[29] Soken, H. E., and Hajiyev, C., "Adaptive Unscented Kalman Filter with Multiple Fading Factors for Pico Satellite Attitude Estimation," *Proceedings of the 4th International Conference on Recent Advances in Space Technologies*, IEEE Publ., Piscataway, NJ, 2009, pp. 541–546. doi:10.1109/RAST.2009.5158254

[30] Cloutier, J., Lin, C.-F., and Yang, C., "Maneuvering Target Tracking via Smoothing and Filtering Through Measurement Concatenation," *Journal of Guidance, Control, and Dynamics*, Vol. 16, No. 2, 1993, pp. 377–384. doi:10.2514/3.21013

[31] Stallard, D., "An Angle-Only Tracking Filter for a Maneuvering Target," *Guidance, Navigation and Control Conference*, AIAA, Reston, VA, 1990; also AIAA Paper 1990-3343. doi:10.2514/6.1990-3343

[32] Bekir, E., "Adaptive Kalman Filter for Tracking Maneuvering Targets," *Journal of Guidance, Control, and Dynamics*, Vol. 6, No. 5, 1983, pp. 414–416. doi:10.2514/3.19852

[33] Lee, H., and Tahk, M.-J., "Generalized Input-Estimation Technique for Tracking Maneuvering Targets," *IEEE Transactions on Aerospace and Electronic Systems*, Vol. 35, No. 4, 1999, pp. 1388–1402. doi:10.1109/7.805455

[34] Park, Y.-H., Seo, J., and Lee, J.-G., "Maneuvering Target Tracking Using the Variable Dimension Filter with Input Estimation," *Astrodynamics Conference*, AIAA, Reston, VA, 1992; also AIAA Paper 1992-4600. doi:10.2514/6.1992-4600

[35] Blom, H. A., and Bar-Shalom, Y., "The Interacting Multiple Model Algorithm for Systems with Markovian Switching Coefficients," *IEEE Transactions on Automatic Control*, Vol. 33, No. 8, 1988, pp. 780–783. doi:10.1109/9.1299

[36] Yun, J., and Ryoo, C.-K., "Missile Guidance Law Estimation Using Modified Interactive Multiple Model Filter," *Journal of Guidance, Control, and Dynamics*, Vol. 37, No. 2, 2014, pp. 484–496. doi:10.2514/1.61327

[37] Helmick, R. E., Blair, W. D., and Hoffman, S. A., "Fixed-Interval Smoothing for Markovian Switching Systems," *IEEE Transactions on Information Theory*, Vol. 41, No. 6, 1995, pp. 1845–1855. doi:10.1109/18.476310

[38] Nandakumaran, N., Sutharsan, S., Tharmarasa, R., Lang, T., McDonald, M., and Kirubarajan, T., "Interacting Multiple Model Forward Filtering and Backward Smoothing for Maneuvering Target Tracking," *Proceedings of SPIE*, Vol. 7445, Signal and Data Processing of Small Targets, International Soc. for Optics and Photonics, Bellingham, WA, 2009, Paper 744503. doi:10.1117/12.826549

[39] Wiesel, W. E., *Modern Astrodynamics*, Aphelion Press, Beavercreek, OH, 2010, pp. 4–13.

[40] Simon, D., *Optimal State Estimation: Kalman, H Infinity, and Nonlinear Approaches*, Wiley, Hoboken, NJ, 2006, Chaps. 2, 14.

[41] Hartikainen, J., Solin, A., and Särkkä, S., *Optimal Filtering with Kalman Filters and Smoothers — A Manual for the Matlab Toolbox EKF/UKF*, Aalto Univ. School of Science, Espoo, Finland, Aug. 2011, pp. 33–34, Ver. 1.3.

[42] McReynolds, S. R., "Fixed Interval Smoothing: Revisited," *Journal of Guidance, Control, and Dynamics*, Vol. 13, No. 5, 1990, pp. 913–921. doi:10.2514/3.25419

[43] Wright, J. R., Woodburn, J., Truong, S., and Chuba, W., "Sample Orbit Covariance Function and Filter/Smoother Consistency Tests," *18th AAS/AIAA Space Flight Mechanics Meeting*, American Astronautical Soc. Paper 2008-159, Springfield, VA, Jan. 2008.

[44] Kelecy, T., and Jah, M., "Detection and Orbit Determination of a Satellite Executing Low Thrust Maneuvers," *Acta Astronautica*, Vol. 66, No. 5, 2010, pp. 798–809. doi:10.1016/j.actaastro.2009.08.029

[45] Williams, J. L., "Gaussian Mixture Reduction for Tracking Multiple Maneuvering Targets in Clutter," M.S. Thesis, U.S. Air Force Inst. of Technology, Wright–Patterson AFB, OH, 2003.